Spatiotemporal Scouring Processes around a Square Column on a Sloped Beach Induced by Tsunami Bores

Alexander Schendel[1]; Stefan Schimmels[2]; Mario Welzel[3]; Philippe April-LeQuéré[4]; Abdolmajid Mohammadian[5]; Clemens Krautwald[6]; Jacob Stolle[7]; Ioan Nistor, M.ASCE[8]; and Nils Goseberg, M.ASCE[9]

Abstract: Tsunamis continue to pose an existential threat to life and infrastructure in many coastal areas around the world. One of the risks associated with tsunamis is the formation of deep scour holes around critical infrastructure and other coastal buildings, compromising their structural integrity and stability. Despite its importance, tsunami-induced scour is still given limited and simplified consideration in design guidelines for coastal structures. To further improve the understanding of tsunami-induced scour processes, and thus provide the basis for safer design of coastal structures, novel large-scale laboratory experiments have been conducted. The experiments featured a unique combination of boundary conditions, including a square coastal structure on a sloping and dry sandy beach. Single broken solitary waves were used to simulate tsunami bores. The spatiotemporal scour development directly at the square column was monitored by a high-resolution camera system, allowing a detailed description of the highly dynamic flow and scour process. Differences in the scour process between the wave runup and drawdown phases are described, and maximum and final scour depths are given as a function of inundation depth, wave height, and distance of the column from the shoreline. The scour process is characterized by several distinct phases of varying intensity and scour rate, the sequence of which varies depending on the location on the sides of the column. It is shown that the drawdown phase has a large influence on the overall scour development, adding up to 58% to the scour depth obtained during the wave runup phase. As a result of significant sediment infilling during the drawdown phase, the maximum scour depths achieved during the drawdown phase are up to twice the final scour depths at the end of a test. This discrepancy between final and maximum scour depths is greater than in previous studies using a flat sediment bed. The results of this study therefore help to interpret scour depths measured during field investigations after a tsunami event and provide a basis for extending design guidelines for coastal structures. **DOI: 10.1061/JWPED5.WWENG-2052**.

Author keywords: Scour; Tsunami; Wave-structure-interaction; Solitary wave; Sediment transport; Laboratory experiments.

Introduction and Motivation

Tsunamis continue to pose an existential threat to lives and infrastructure in many coastal areas around the world. Numerous studies have been conducted in recent decades to understand the risks and eventually mitigate hazards resulting from tsunamis (Nouri et al. 2010; Palermo et al. 2013; Nistor et al. 2017; Stolle et al. 2018a; Krautwald et al. 2021). One of these risks is the emergence of deep scour holes around critical infrastructures, affecting their structural integrity and stability. Moreover, buildings undermined by scour may no longer be suitable for evacuation purposes. In recent years, field studies following the 2011 Tohoku tsunami and the 2018 Indonesia tsunami have provided new insights into the mechanisms of tsunami-induced scour and its threat to the stability of coastal defense structures.

Following the 2011 Tohoku tsunami, Bricker et al. (2012) conducted scour measurements at four sites in Chiba and Fukushima prefectures, Japan. Their study focused on scour behind seawalls

[1]Research Associate, Ludwig-Franzius-Institute for Hydraulic, Estuarine and Coastal Engineering, Leibniz Universität Hannover, 30167 Hannover, Germany; Coastal Research Center, Joint Research Facility of Leibniz, Universität Hannover and Technische Universität Braunschweig, Hannover, Germany (corresponding author). ORCID: https://orcid.org/0000-0003-4938-1062. Email: schendel@lufi.uni-hannover.de

[2]Coastal Research Center, Joint Research Facility of Leibniz Universität Hannover and Technische Universität Braunschweig, 30419 Hannover, Germany.

[3]Research Associate, Ludwig-Franzius-Institute for Hydraulic, Estuarine and Coastal Engineering, Leibniz Universität Hannover, 30167 Hannover, Germany.

[4]Dept. of Civil Engineering, Univ. of Ottawa, 161 Louis-Pasteur Private, Ottawa, ON, Canada K1N 6N5.

Note. This manuscript was submitted on August 11, 2023; approved on January 17, 2024; published online on March 21, 2024. Discussion period open until August 21, 2024; separate discussions must be submitted for individual papers. This paper is part of the ***Journal of Waterway, Port, Coastal, and Ocean Engineering***, © ASCE, ISSN 0733-950X.

[5]Professor, Dept. of Civil Engineering, Univ. of Ottawa, 161 Louis-Pasteur Private, Ottawa, ON, Canada K1N 6N5.

[6]Research Associate, Leichtweiß-Institute for Hydraulic Engineering and Water Resources, Dept. of Architecture, Civil Engineering and Environmental Sciences, Technische Universität Braunschweig, Beethovenstr. 51a, 38106 Braunschweig, Germany. ORCID: https://orcid.org/0000-0001-8928-1352

[7]Associate Professor, Eau Terre Environment, INRS, 490, Rue de la Couronne, Québec City, QC, Canada G1K 9A9. ORCID: https://orcid.org/0000-0003-0902-9339

[8]Professor, Dept. of Civil Engineering, Univ. of Ottawa, 161 Louis-Pasteur Private, Ottawa, ON, Canada K1N 6N5. ORCID: https://orcid.org/0000-0001-8436-4781

[9]Professor, Dept. of Architecture, Civil Engineering and Environmental Sciences, Technische Universität Braunschweig, Beethovenstr. 51a, 38106 Braunschweig, Germany; Coastal Research Center, Joint Research Facility of Leibniz, Universität Hannover and Technische Universität Braunschweig, Hannover, Germany. ORCID: https://orcid.org/0000-0002-1550-3001

and at building foundations, where the maximum scour depth was found to be 2 m. The need for further studies was highlighted by a comparison with several analytical and empirical approaches to predict tsunami-induced scour that showed considerable deviations between observations and predicted scour depth. The consequences of the same tsunami event on the stability of coastal structures have also been described by Jayaratne et al. (2016). The authors conducted field surveys in Miyagi and Fukushima prefectures, Japan, to investigate the failure mechanisms of coastal structures, and leeward toe scour was recognized as the main failure mechanism at most of the sites surveyed. In addition, Yeh et al. (2013) found evidence of seawall failure due to scour during tsunami return flow after the 2011 Tohoku tsunami. As a possible explanation for the severe scour during return flow, the authors hypothesize a decrease in soil stability due to the development of a pore pressure gradient caused by the rapidly decreasing inundation depth. Finally, Krautwald et al. (2021) reported on scour mechanisms and corresponding damage to buildings in Palu City, Indonesia, due to the large tsunami event in 2018. In their field survey, they found evidence of scour around buildings due to sustained and channelized flow, as well as plunging scour behind seawalls. The authors also identified floating debris as a potential cause and entry point for scour. These studies, along with many earlier ones, show the impact of a tsunami on coastal infrastructure and clearly demonstrate the importance of scour as a dominant cause of failure for many structures.

Despite its importance in assessing the overall performance of buildings with respect to natural hazards, scour induced by extreme hydrodynamic events is only given limited and, to date, simplified consideration in foundation design guidelines (ASCE7-22 Chapter 6; ASCE 2022). This can partly be attributed to challenges related to physical and numerical simulation as well as in situ observations. Experimental methods are often tied to small length scales while numerical simulations often must resort to single-phase models, as multiphase methods remain computationally expensive. In situ observations are notoriously challenging as tsunami predictions are still not possible, and hence, instrumentation of potential sites remain out of reach. Consequently, in situ observations only show the aftermath, but cannot provide insight into the scour processes during a tsunami event, and therefore often underestimate the scour depths, which are partially refilled toward the end of the drawdown phase due to the high sediment load carried by the return flow. However, before the scour hole is refilled, large erosion can occur around the onshore face of the structures because of the return flow (Tonkin et al. 2003). This severe erosion process is in parts driven by momentary liquefaction (Yeh and Mason 2014). During the inundation of the tsunami, water infiltrates the soil below the rising water level, causing the pore pressure in the soil to increase. If the water level decreases rapidly as the tsunami recedes, the soil does not have enough time to drain and dissipate the pore pressure. As a result, an upward-directed pore pressure gradient is established, reducing the effective stress in the soil (Tonkin et al. 2003; Benjamin Mason and Yeh 2016). For a better understanding of the full damage potential of tsunami-induced scour, the transient scour process must be considered over its entire duration, including the drawdown phase, and spatial extent.

In large-scale experiments, Yeh et al. (2001) examined the scour development around a cylindrical structure standing on a sloped (1:20) sandy beach. Solitary waves were used to model a tsunami and the scour process around the cylinder was recorded by video cameras. Tonkin et al. (2003) completed their study with tests that incorporated an additional gravel collar around the cylinder. In their detailed discussion of the transient flow and scour process, Tonkin et al. (2003) included the drawdown phase, during which the greatest scour depth occurred on the onshore side of the cylinder. The authors explained the rapid and deep scour at this location by the additional upward excess pore pressure gradient, and consequently, reduced frictional resistance of the sediment grains to erosion. In their experiments, an excess pore pressure gradient equal to only about one-half of the buoyant specific weight of the saturated sand was found to be sufficient to greatly increase the scour development. Liquefaction, the state when the excess pore pressure exceeds the buoyant specific weight of the soil, was not reached. The description of scour evolution over time was restricted to three positions around the cylinder and data from only three test cases were shown. In extensive laboratory and numerical experiments, Nakamura et al. (2008) studied scour formation around a square structure located behind a revetment on a flat sand bed. Both solitary and isolated long waves were generated and generally greater final scour depths were found for the case of the isolated long waves. For those tests, a video camera was used to record the scour process at one of the offshore corners. For that location, it was shown that the maximum scour depth during the tsunami overflow can be significantly greater than the final scour depth due to sediment settlement with decreasing flow velocities. The effects of the drawdown phase of a tsunami wave were not considered.

In another set of experiments, McGovern et al. (2019) used a pneumatic long wave generator to generate tsunami waves with periods between 25 and 147 s, allowing the effect of inundation depth, duration, and Keulegan-Carpenter (KC) number on scour around a square structure to be assessed. The transparent structure was placed on a flat sediment bed. It was shown that the scour depth around the square structure can vary significantly during the tsunami runup, which may indicate that an equilibrium state has not yet been reached. Furthermore, the duration of the inundation appeared to be a more important driver of the maximum scour depth, which was significantly reduced toward the end of the inundation due to sediment slumping rather than the inundation depth. More recently, Mehrzad et al. (2022) used hydraulic bores to simulate tsunami-induced scour around a square structure. In three tests with different inundation depths, the bores were generated using the dam break method by rapidly opening a swing gate. The square structure was placed on a dry and flat sand bed. A detailed description of the vortex structure, flow field, and temporal scour development was obtained by video recording. The results showed a strong dependence of scour depth on bore depth and maximum scour depths significantly greater than predicted by previous studies and guidelines. However, without modeling the drawdown phase, the maximum local scour depth occurred at the offshore corner and scour at the onshore corner was insignificant. But even without return flow, and similar to what was observed by McGovern et al. (2019), the final scour depth was substantially smaller than the maximum scour depth during the bore runup due to slumping of the scour hole slopes and sediment infilling.

For tsunami-induced local scour around a land-based structure, previous studies have shown that the scour process is influenced by a multitude of parameters such as sediment properties (Lavictoire 2014), structural geometry (Mehrzad et al. 2016), flow depth (Tonkin et al. 2013), wave period (McGovern et al. 2019), or varying boundary layer dynamics of the tsunami wave (Larsen et al. 2018). However, most studies consider tsunami-induced scour around a coastal structure on horizontal terrain. This means that the drawdown phase of the tsunami wave is not considered, although the scour development during this second flow phase can be significant (Tonkin et al. 2003; Yeh et al. 2013). The mechanisms controlling the transient scour development throughout the duration of the tsunami inundation, as well as the sediment transport processes leading to the partial refilling of the established

scour hole, are not fully understood. To determine whether and to what extent the dynamic sequence of drawdown contributes to the scour depth, the scour development during the entire runup and drawdown phase needs to be systematically evaluated. In addition, many previous studies only provide a partial picture of the spatial scour process at certain positions along the studied structure, which means that, for example, sediment deposition and transport processes within the scour hole, as known from similar transient tidal currents (Schendel et al. 2018), cannot be captured. Large-scale model tests, which provide a "full picture" of the scour process in space and time, can therefore make a valuable contribution to the understanding of tsunami-induced scour and thus to the safety of coastal regions.

To this end, the novel large-scale model tests presented in this study were carried out with a unique combination of boundary conditions, including a sloping and dry sand beach, a square coastal structure, and high temporal and spatial resolution capture of flow and scour processes. In this study, the term "spatial scour development" refers to the near-field scour process along the sides of the structure, rather than a far-field global scour pattern. This study aims to improve the understanding of the time-variant scour process induced by single broken solitary waves at large scale. When compared with similar previous studies such as the ones carried out by McGovern et al. (2019) or Mehrzad et al. (2022), which also adopted a square structure, the novelty of this research rests in the meticulous evaluation and comparison of flow and scouring phenomena occurring during the drawdown as well as runup phases, using large-scale experiments. The series of experiments also included the investigation of the influence of successive individual waves on the development of scour, as may occur in natural tsunami events. This aspect will be discussed in detail in a follow-up publication and is a novelty compared with previous studies.

The specific objectives of this study include:

1. To obtain and report a novel data set, with a focus on high-resolution acquisition of flow and spatiotemporal evolution of the scour processes around a square column including the drawdown phase.
2. To compare and to understand the development of maximum scour depths at selected instants during tsunami inundation as a function of the wave height and distance from shore.
3. To advance the knowledge on tsunami-induced scour by minimizing prediction uncertainties by large-scale laboratory experiments.

As part of a broader investigation pertaining to understanding the scouring processes around square columns located on inclined beaches, a subset of laboratory tests has already been addressed in April-LeQuéré et al. (2022). April-LeQuéré et al. (2022) used a state-of-the-art numerical model (FLOW-3D) to numerically reproduce the experimental results, but focused mainly on the flow and turbulence structure around the column, the intensity of which differed greatly between the runup and the drawdown flow phases. The numerical model showed an accurate representation of the flow characteristics of the wave runup on the sloping beach and around the square column but underestimated the large scour on the onshore side of the column. April-LeQuéré et al. (2022) considered scour development either at specific times or at individual specific locations for a selected test case. This paper continues the authors' analysis and now concentrates on an in-depth analysis of the experimental results, looking at scour development over the entire circumference of the square column over time, an analysis previously overlooked in the recent literature. For consistency and legibility, some information already provided in April-LeQuéré et al. (2022) on the experimental layout and methodology are reiterated.

Material and Methods

Experimental Facility

The study was carried out in the Large Wave Flume (GWK) of the Coastal Research Centre, Germany. The GWK is 307 m long, 5 m wide and 7 m deep. Waves are generated by a piston-type wave generator with a usable stroke for wave generation of ± 2.0 m. Regular waves up to a height of 2.10 m and wave spectra with a maximum significant wave height of $H_s = 1.3$ m can be generated under prototype conditions (Schendel et al. 2015; Gieschen et al. 2021). Furthermore, the wave maker can filter re-reflections by an active absorption system.

In accordance with the experiments conducted by Tonkin et al. (2003), a beach with a slope of 1:20 was built, the toe of which started 170 m from the wave maker. The slope was made of sand with a median diameter $d_{50} = 0.345$ mm, a geometric standard deviation of $\sigma_g = \sqrt{d_{84}/d_{16}} = 1.50$, a void ratio $e = 0.77$, and a density of $\rho_s = 2.65$ g/cm^3. The coefficient of uniformity (C_u) was 1.87, the coefficient of curvature (C_c) 1.11, and the permeability test resulted in a saturated hydraulic conductivity of $K_s = 0.333$ cm/s.

Column Model and Setup

A square acrylic column was installed on the beach and above the still water level (SWL). The column had a width of 0.6 m, a total height of 2.2 m, and reached about 1.0 m below the surface of the beach, from where it was fixed to a heavy concrete substructure via a steel construction. The ballast of the sand provided the necessary stability for the foundation of the column. The sand was brought in with heavy equipment (wheel loader) and compacted at the same time. First, the sand was installed up to the column position. After the column was placed, the rear part of the beach was completed. To guarantee a good compaction and to reduce entrapped air, the sand around the column was washed in with water. The column was positioned in the center of the beach and the influence of the blockage on the flow is assumed to be negligible as the blockage ratio of column width to flume width (0.6 m/5.0 m = 0.12) lies below the critical threshold of 1:6 as suggested by Whitehouse (1998). Detailed information about the experimental setup is shown in Fig. 1.

Measurements and Instrumentation

Along the large wave flume and close to the position of the square column, a set of instruments was installed to record relevant flow properties and to closely observe the spatiotemporal evolution of the scour whose positions are provided in Fig. 1. Flow velocities were measured by two acoustic Doppler velocimeters (ADVs; Nortek 3D, Vector) and, for redundancy, two electromagnetic current meters (ECMs; HS Engineers, ISM 2001) were added. The ADVs were mounted at a height of 0.05 m, whereas the ECMs were placed 0.15 m above the initial sand level. On opposite sides of the flume, the ADVs and ECMs were installed 0.9 m upstream and downstream of the longitudinal location of the column's center, at a distance of 0.6 m from the flume walls. During the analysis, it became apparent that the data quality of the ADVs was affected by the high turbulence, the high air content, and the low water level over long periods of the wave runup. It was therefore decided not to use the data of the ADVs for analysis and result interpretation at this time.

Up to the toe of the beach, the water surface elevation was recorded by eight resistance-capacity wave gauges (custom-made,

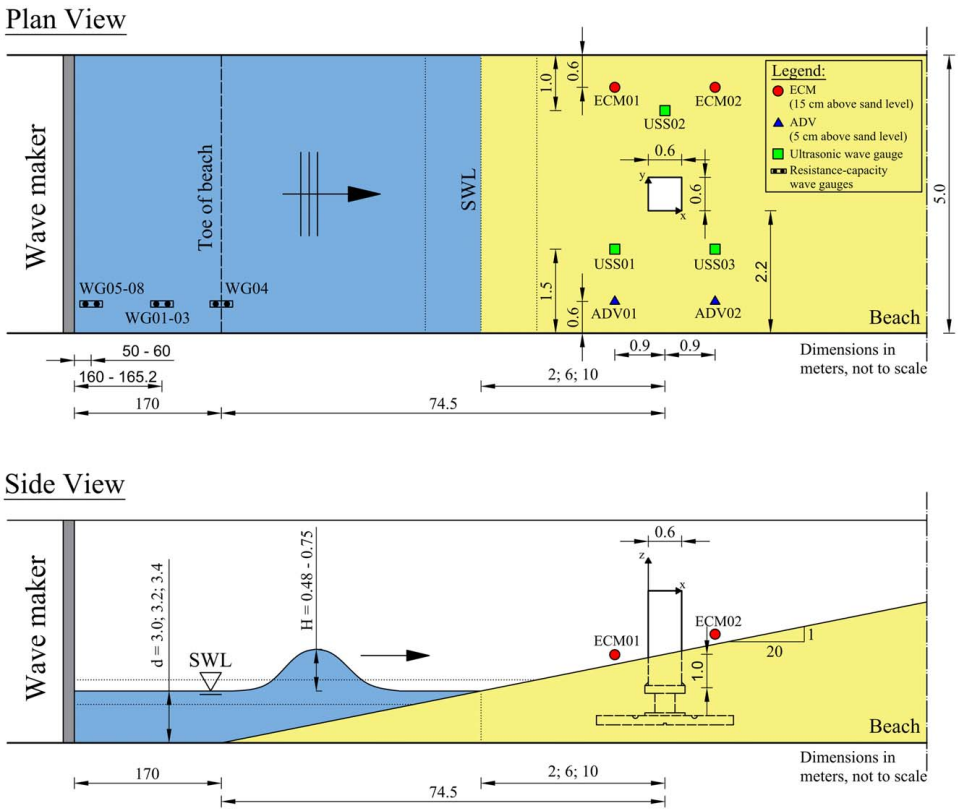

Fig. 1. Experimental setup in plan and side view.

accuracy of wave height measurement ±5 mm). On the beach, three ultrasonic wave gauges (USS, Microsonic 340, ±1% accuracy with a resolution of 0.18 to 1.5 mm) were used to measure the water surface elevation close to the column. To allow an estimation of the flow depth around the column and a direct comparison with the flow velocity measurements, two ultrasonic sensors (USS01 and USS02) were placed on the same axis as the ECMs, while the third ultrasonic sensor (USS03) was located on the same axis as the center of the column. The lateral distances of USS01 and USS02 from the column were 0.4 m, while USS03 was 0.9 m from the column. Fig. 2 shows the transparent column and the position of the measurement devices around it. Data acquisition of all flow velocity and water surface elevation measurements was bundled into a single data collection system with a sampling rate of 100 Hz.

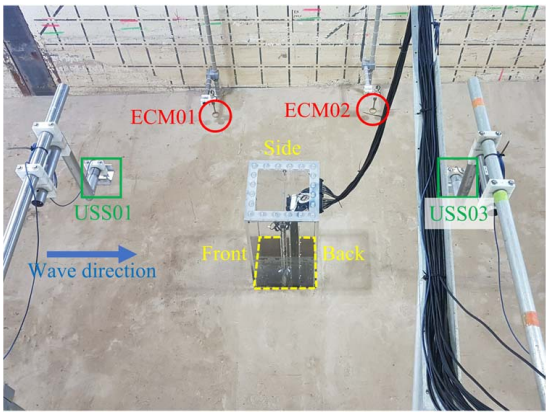

Fig. 2. Square column and overview of measuring setup.

The spatiotemporal scour development directly at the column was monitored by a camera system placed inside the transparent column, while the spatial scour pattern in the vicinity and the far field was measured using a 3D laser scanner (Faro Focus 3D) between individual tests. The camera system inside the column consisted of four GoPro (GoPro Hero 8) of which two were arranged on top of each other.

Two of the cameras looked at the offshore face ("front") and one side face ("side") of the column, while the other two cameras looked at the onshore face ("back") of the column and the same side face, fully covering three sides of the column. Since the experimental setup was symmetrical in the direction of wave runup, a symmetrical scour pattern was expected, assuming that coverage of the scour along three sides of the column should be sufficient to capture the scour process. Each GoPro was controlled individually via remote access. The synchronization of the cameras with each other and with the rest of the measuring equipment was accomplished visually by means of an LED in the field of view of the cameras, which was automatically switched on at the start of the measurement.

To extract scour depths from the camera images, the optically distorted images were corrected. For this purpose, lens distortion was removed using the intrinsic parameters of the cameras determined by a checkerboard calibration. Subsequently, predefined reference points on the column were identified and the undistorted image was transformed from pixel coordinates to real-world distances (Stolle et al. 2016). An example showing the original picture taken by one of the GoPro as well as the final transformed pictures is given in Fig. 3.

From the transformed images, spatial scour depths along the column were manually determined at selected time intervals. The originally envisaged automated acquisition of scour depths from the camera images did not provide continuously satisfactory results due to the high sediment load (Fig. 3) and the occasional poor

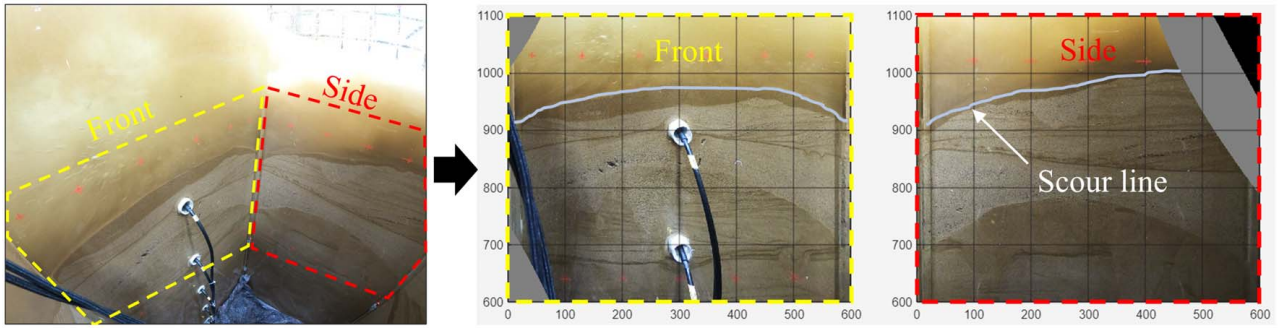

(a) (b)

Fig. 3. (a) Original picture taken by one of the GoPros; and (b) transformed pictures at the front and side face of the column, converted to real-world coordinates and dimensions in millimeters.

distinguishability between fluid and solid bed. The sampling rate of the GoPros was set to 24 fps at a resolution of 3,000 × 4,000 pixel, resulting in a practical accuracy for the scour depth measurements of <1 mm on average after image transformation. However, the accuracy of the scour depth readings was affected by high turbulence in the water phase, characterized by substantial suspended sediment transport, so that only scour measurements are used for which a clear distinction between fluid and sediment phase could be made.

Hydraulic Conditions, Test Program, and Procedures

To mimic a tsunami event, a choice of solitary waves was generated with a nonlinearity parameter (H/d) between 0.15 and 0.24 and wave periods between 7.6 and 10.1 s. The wave period was derived from wave gauge measurements at the toe of the beach and is consistent with the definition of McGovern et al. (2019) according to which a water surface elevation equal to 1% of the wave amplitude has been exceeded.

The change of the nonlinearity parameter was achieved by adjusting the wave height (H) as well as the water depth (d) between tests. With the change in water depth, the distance of the column from the SWL varied too, which had been included as an important experimental parameter. The distance of a structure to the shoreline will inevitably, and in agreement with April-LeQuéré et al. (2022), lead to variations in the approaching flow field and this is the prime parameter which controls sediment stirring and initiation of sediment transport.

A total of five test setups were conducted, in which each wave was repeated three to four times to simulate the influence of several consecutive tsunami runups. In this study, however, only the development of scour as a result of the first waves will be addressed. As described in Schimmels et al. (2016), the solitary waves were generated using the method of Goring (1978). An example of the offshore water surface elevation of a generated solitary wave (Test T02b) is given in April-LeQuéré et al. (2022), showing a good agreement with the analytical approach at the toe of the beach (wave gauge WG04 in Fig. 1). Test conditions and scour depths for all tests are summarized in Table 1.

The observed flow velocities at the time of wave impact on the column were high and could not be reliably captured by the ECM probes in the first few moments. Furthermore, since the ECM probes could only measure flow velocities at flow depths > 15 cm, usable flow velocities measurements were only available in a short time window before and after the flow reversal when reverting from runup to drawdown. However, the flow velocities in this time window are, by their nature, comparatively small and thus unlikely to be representative of the actual load throughout a test. To overcome the shortcoming of the flow measurements and provide representative flow parameters, the time history of flow velocities over the entire test duration were appended numerically by means of a FLOW-3D model. A comprehensive description of the FLOW-3D model can be found in April-LeQuéré et al. (2022), in which it was utilized for both the simulation of scour and the hydrodynamics of the bore, including the turbulent flow structure around the column. Fig. 4 compares the measured with the simulated flow depth for the three tests with identical water depth but different wave height, and Fig. 5 juxtaposes the measured and simulated flow velocities for the same tests. To improve comparability between the measured and modeled time series, the time series were shifted so that the time of flow reversal is set as zero.

The comparison shows a generally good agreement between simulated and measured flow data. Flow depths are slightly overestimated by the numerical model after flow reversal, especially upstream of the pile (USS01), whereas flow velocities are slightly underestimated during reverse flow. For all tests, an average coefficient of determination R^2 of 0.89 could be determined for the comparison of flow velocities and an R^2 of 0.57 for the flow depth comparison. For a selected test, April-LeQuéré et al. (2022) showed that the FLOW-3D model could reproduce the measured scour depth and pattern reasonably well. Therefore, the simulated flow depths and flow velocities will be used in the following to describe the hydrodynamic loading and flow regimes during the tests. However, while the simulated flow conditions can help to understand general dependencies and processes, they are unlikely to explain individual, local and short-term differences in scour depth between tests.

Accordingly, the Froude (Fr), the Reynolds (Re), the KC numbers, and the momentum flux (M) in Table 1 are based on the simulated flow values as

$$\mathrm{Fr} = \max\left(\frac{\bar{U}_i}{\sqrt{g h_i}}\right) \tag{1}$$

$$\mathrm{Re} = \max\left(\frac{h_i \bar{U}_i}{\nu}\right) \tag{2}$$

$$\mathrm{KC} = \frac{\max(\bar{U}_i) T}{D} \tag{3}$$

$$M = \max(h_i \bar{U}_i^2) \tag{4}$$

$$\text{for } t_{\text{reverse}} \le i \le t_{\text{end}}$$

Table 1. Test conditions and scour depths obtained in tests with structure

Test	Water level d [m]	Wave height H [m]	Nonlinearity parameter H/d [–]	Distance SWL W [m]	Wave period T [s]	Depth-averaged flow velocity $\bar{U}_{max}$ [m/s]	KC number KC [–]	Reynolds number Re [–] $\times 10^5$	Froude number Fr [×]	Shields parameter θ [–]	Momentum flux M [m^3s^{-2}]	Final scour depth S_{end}/D [–]	Maximum scour depth S_{max}/D [–]	Scour depth at flow reversal $S_{reverse}/D$ [–]
T01b	3.0	0.728	0.243	10	7.65	1.98	25.25	2.88	2.32	2.20	0.49	0.160	0.278	0.207
T02b	3.2	0.738	0.230	6	10.10	2.23	37.54	3.50	2.24	2.68	0.74	0.188	0.323	0.271
T03	3.2	0.482	0.151	6	8.27	1.80	24.81	2.87	2.29	1.89	0.42	0.159	0.322	0.203
T04	3.2	0.616	0.193	6	7.63	2.02	25.69	2.88	2.29	2.29	0.54	0.176	0.265	0.253
T05	3.4	0.746	0.219	2	7.68	2.32	29.70	3.88	2.32	2.85	0.83	0.232	0.367	0.361

Note: The flow parameter KC, Re, Fr, θ, and M are based on FLOW-3D simulation results at the position of ECM02 and during the rundown stage. The flow velocity U_{max} represents the maximum flow velocity during the rundown phase.

where g = gravitational acceleration; h = flow depth; ν = kinematic viscosity; t = time during a test; T = wave period; D = width of the square column; $\bar{U}$ = depth-averaged flow velocity at the position of ECM02 obtained by FLOW-3D simulation (April-LeQuéré et al. 2022). Instead of using the flow velocity at the level of the ECM measurement (15 cm above the bottom), the depth-averaged flow velocity was chosen as a reference value over the entire duration of the test. The flow parameters (KC, Re, Fr, θ, M) represent the maximum value during the wave rundown stage, starting with treverse and ending with t_{end}.

The Shields parameter (θ) was calculated as in Tonkin et al. (2003) using the definition of Hoffmans and Verheij (1997). In this approach, a current induced Shields parameter is determined based on the assumption of a logarithmic velocity profile and a bed roughness $z_0 = d_{90}/d_{30}$.

The procedure for each series of tests can be described as follows:

1. Perform a reference measurement of the undisturbed bathymetry and topography of the beach with the 3D laser scanner.
2. Fill in water to the desired water level and run a test with a single solitary wave.
3. Wait until the area around the column has dried and perform measurements of the spatial scour pattern by using the 3D laser scanner.
4. Generate the next single solitary wave and repeat step 2. In all tests, four individual solitary waves have been generated, except in Test T05 where only three were generated.
5. Lower the water level to allow for a full reconstruction of the beach slope and wait for the water inside the beach to seep back to the sea water line (usually about 12 h overnight).
6. Reconstruct the initial level of the sand bed.
7. Repeat this process for the next test with new wave parameter.

Results

Flow and Scouring Processes Induced by Tsunamis

Similar to the descriptions in Mehrzad et al. (2022) and McGovern et al. (2019), a detailed overview of the flow and the resulting scouring processes at the column will be provided first to illustrate the hydrodynamic conditions, prior to more complex analyses.

The flow processes observed in the experimental runs clearly differ from those described in previous studies in that uniquely, due to the beach slope, a gravity-driven return flow occurred during which the flow interacts with the column differently from that during wave runup, causing significant scour development on the downstream side of the column as will be described below. The description of the flow and scouring processes is exemplarily carried out on the basis of Test T03 ($H/d = 0.151$, $W =$ 6 m).

Based on the video recording from inside the column, Fig. 6 shows the flow around the column for selected instances in time. Time $t = 0$ describes the time of impact of the bore on the column. With respect to this reference time, the flow reversal between runup and downflow took place at about $t = 6.8$ s.

1. $t = 0.25$ s (Fig. 6a): the turbulent, broken bore hit the column at high velocity (> 7 m/s, as determined by visually tracing the bore front along the lateral face of the column) and ran upward of the upstream (front) face of the column. The flow at the upstream face showed similarities to a wall jet described by Rivière et al. (2017) for an obstacle in supercritical open-channel flow. By means of the wall jet, the deflection of the flow around

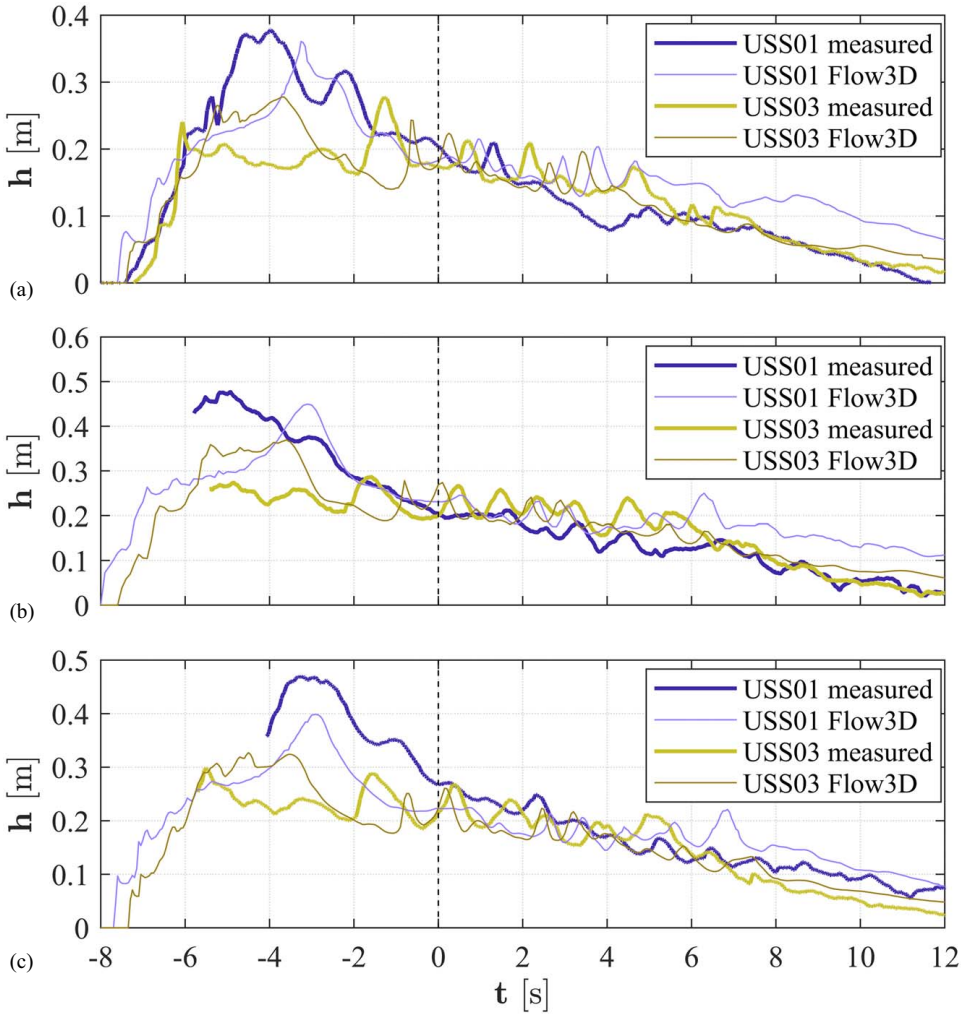

Fig. 4. Comparison of measured and simulated (Flow3D) flow depth at the position of USS01 and USS03 for (a) Test 03; (b) Test 02b; and (c) Test 04.

the obstacle, formed by the column, is partly performed outside the main flow, without the need for a horizontal streamline curvature. A smaller vertical runup of the flow onto the upstream face of the column was also reported in Mehrzad et al. (2022). Beneath the upshooting wall jet, the flow was very turbulent and turbid, and water rapidly penetrated the dry soil and began to erode sediment along the entire length of the upstream face. Tonkin et al. (2003) reported a rapidly developing scour hole at the offshore face of a cylinder 0.25 s after wave impact. They attributed the scour development to a horseshoe-type vortex, which, however, did not result from the boundary layer separation as in steady flow, but which was induced by the plunging breaker as the wave broke directly at the offshore face of the cylinder. Owing to the high turbidity, a horseshoe-like flow structure could technically not be observed in this study at this point in time. At the lateral face (side), the flow rushed past the column without any significant interaction with the dry sediment or even scour. On the downstream side (back side) the water propagated past the edges of the column at high velocity, leaving the leeward side of the column still completely dry, due to a sheltering effect of the column.

2. $t = 2.00$ s (Fig. 6b): flow depth on both the upstream and the lateral sides increased rapidly, with flow depth on the upstream side remaining clearly the deepest overall. As reported in McGovern et al. (2019), the formation of lateral vortex shedding at the upstream corners of the column resulted in an extensive scour development at this location. From the upstream corners, the eroded sediment was subsequently transported downstream along the lateral face of the column. Contrary to the observations of McGovern et al. (2019), there was no inherent delay in scour development along the centerline of the upstream face. However, the scour process at this location was significantly slower than at the corners. Furthermore, the sediment at the upstream face was transported from the centerline toward the corners. McGovern et al. (2019) argue that the delay indicates that the horseshoe vortex in not likely to be a strong influence on the early stages of scour process. In this study, however, scour took place over the whole upstream face from the initial moment of bore impact, although not with the same intensity everywhere along the front face. Nevertheless, this could indicate a slightly stronger manifestation of the horseshoe vortex and downflow as in McGovern et al. (2019), especially since the seepage flow had already penetrated the sediment layer by about 3 cm below the new bed surface at that time. Given the rapidly decreasing Fr number, the wall jet at the upstream face of the column had also developed into a detached hydraulic jump at this time. A similar hydraulic jump or surface roller was reported in Mehrzad et al. (2022) or observed in Stolle et al. (2018b) for a debris damming in unsteady supercritical flow. The hydraulic jump was deflected in a large curvature around

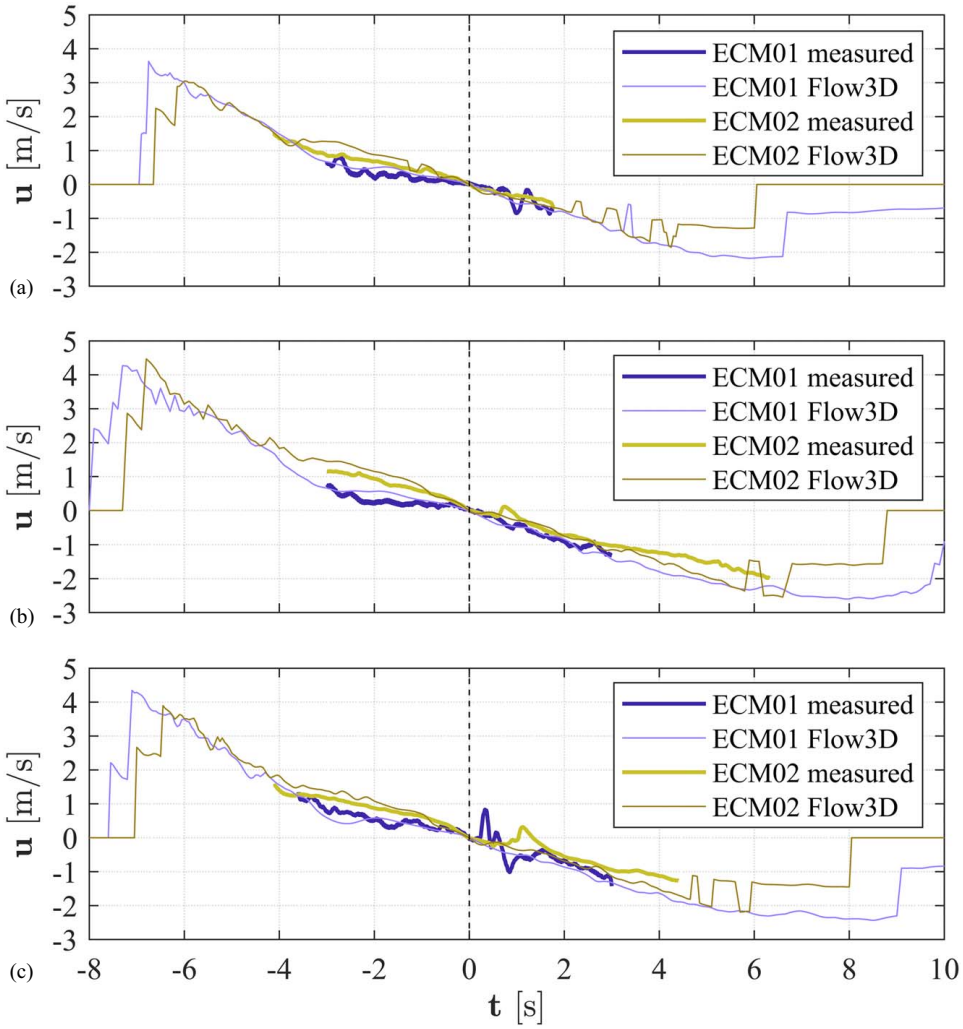

Fig. 5. Comparison of measured and simulated (Flow3D) flow velocities, 15 cm above the bed, for (a) Test 03; (b) Test 02b; and (c) Test 04.

the column and pushed away from the sides of the column. On the downstream side, the bore previously separated by the column started to converge again but had not yet fully converged toward the column.

3. $t = 4.00$ s (Fig. 6c): while the hydraulic jump was diminishing at the upstream side of the column, the flow depth was still considerably larger than on the lateral sides or the downstream side. In addition, the flow became less turbulent and carried less suspended sediment. The flow separation and resulting lateral vortices at the upstream corner of the column resulted in a difference in scour depth between the lateral and downstream parts of the corner. In contrast to the upstream corner, where scour depth continued to increase, the scour process at the centerline of the upstream face was very slow and had nearly halted at this point. From the upstream corner the scour progressed toward the downstream corner. While large erosion took place over the entire length of the lateral face, sediment accumulated on the downstream side (back), leading to small but distinct step in the scour depth at the downstream corner [indicated by the circle in Fig. 6(c)]. On the back of the column, the water rushed from the convergence point of the bore toward the back face of the column. In the process, a large amount of sediment was transported by the flow, leading to the sediment deposition mentioned previously.
4. $t = 6.50$ s (Fig. 6d): shortly before the flow reversal (at $t = 6.8$ s), flow velocities already significantly reduced and flow depths directly at the column had almost equalized. As a result, scour development came to a halt on all sides of the column. On the downstream side of the column, the water column has now completely merged, creating a backflow toward the column. In interplay with the remaining runup flow along the sides of the column, this backflow caused the formation of temporary vortices trailing from the downstream corners of the column.
5. $t = 9.80$ s (Fig. 6e): three seconds after the flow reversal, a hydraulic jump begun to form at the back of the column as a result of the increasing drawdown flow. Similar to the flow processes at the upstream face of the column during wave runup, the flow was diverted from the centerline of the back face toward its corners. The return flow was not yet strong enough to cause erosion at the centerline of the back face. The flow separation and lateral vortices forming at the back corners, however, led to scouring here, analog to the flow and scouring process at the front corners during bore runup. A wall jet did not develop due to lower flow velocities and thus Fr numbers compared with the runup phase. At the same time, the flow depth continued to decrease at the lateral and forward side of the column, where small trailing vortices led to a slight refilling of the scour at the corners.
6. $t = 13.00$ s (Fig. 6f): further reduction of flow depth at the lateral and forward face of the column, while the drawdown flow was still pushing against the back face, increasing the strength of the hydraulic jump. Given the large flow depth and strong

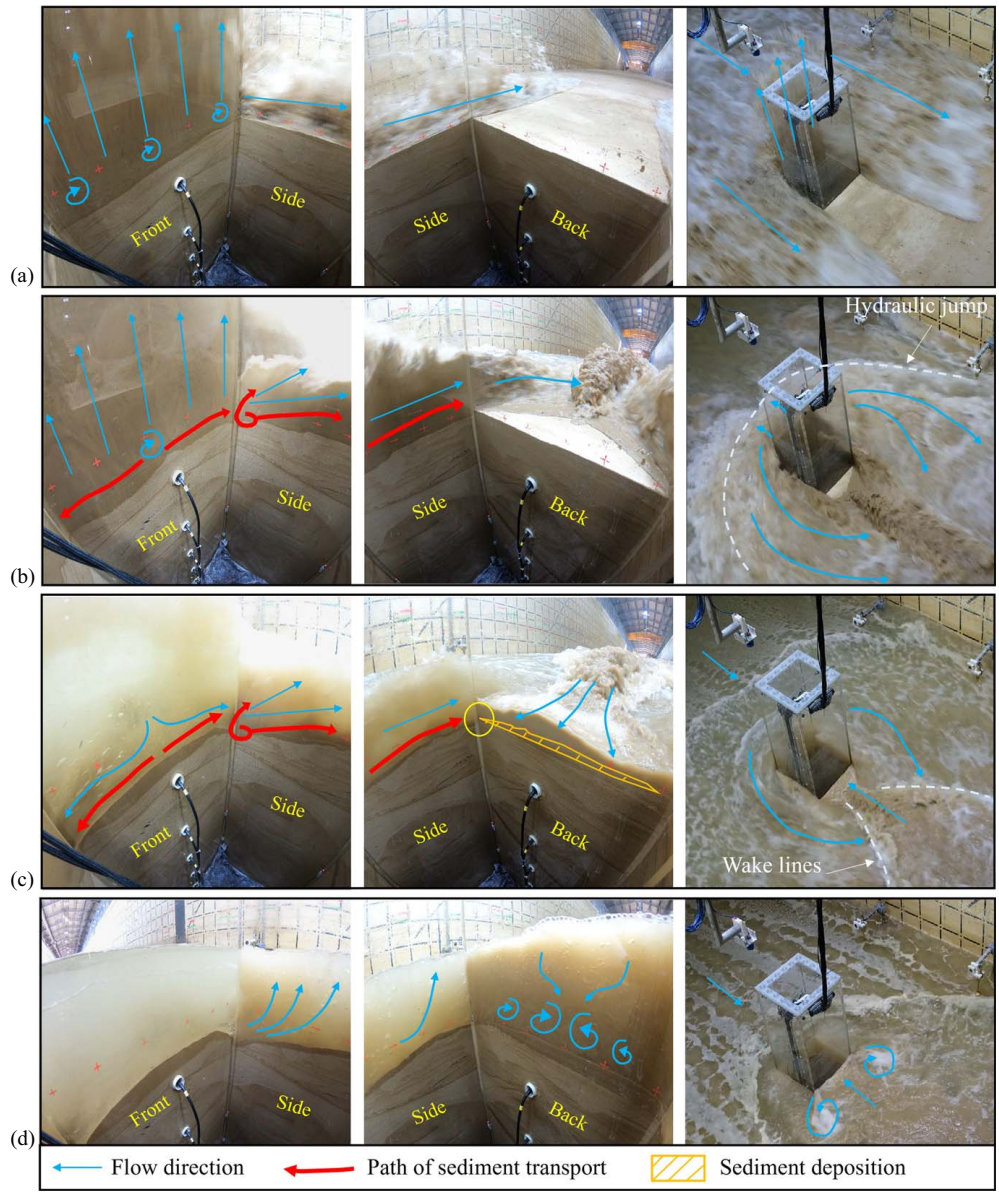

Fig. 6. Flow and scouring processes around the column during Test T03 for selected points in time. Time stamps refer to the moment after the incoming wave hit the column's back face. Shown are the processes after (a) $t = 0.25$ s; (b) $t = 2.00$ s; (c) $t = 4.00$ s; (d) $t = 6.50$ s after wave impact on the column; (e) $t = 9.80$ s; (f) $t = 13.00$ s; and (g) $t = 21.00$ s after wave impact on the column.

downward flow (horseshoe vortex) at the back face of the column, the formation of a downward pore-water pressure gradient is likely at this point. Upward pore pressure gradients, which might result in liquefaction and enhance the scour process as described by Tonkin et al. (2003) are likely to build up at the lateral and forward face of the column, as flow depths were sinking rapidly here. This may partly explain the increasing scour depth in the center of the lateral side. At the same time, the strong return flow caused sheet flow conditions with high sediment mobility along the lateral side. The sediment was pushed along the side, increasing the scour depth in the center of the lateral face but partially refilling the former scour holes at the front corners. At the back face, the downward flow has increased in strength, leading to modest scour at the center and significant scour at the corners of the back face of the column. In addition, flow separation and lateral vortices at the back corners of the column were clearly visible. At the front face, only a small amount of sediment was eroded as the large eddies that formed at the front corners kept sediment in suspension but were not strong enough to cause a larger scour development.

7. $t = 21.00$ s (Fig. 6g): toward the end of the rundown, the water depth decreased rapidly and the hydraulic jump at the back face of the column diminished. However, the flow velocity was still substantial, and a large amount of sediment was transported in sheet flow-like conditions toward the column from more elevated areas of the sloped beach. The high flow velocity resulted in extensive scour development at the back corners of the column, which at the time of its greatest depth exceeded even the scour at the front corners. However, as the flow velocity decreased in the following seconds, the erosion potential at this location gradually became exhausted and the deep scour holes at the back corners were partially refilled by the settling sediment. The rapid scour development at the back of the column may have been supported by an upward pore-water pressure gradient that has eventually set in as the flow depth rapidly decreased. The partially refilling of scour holes at the back and the lateral

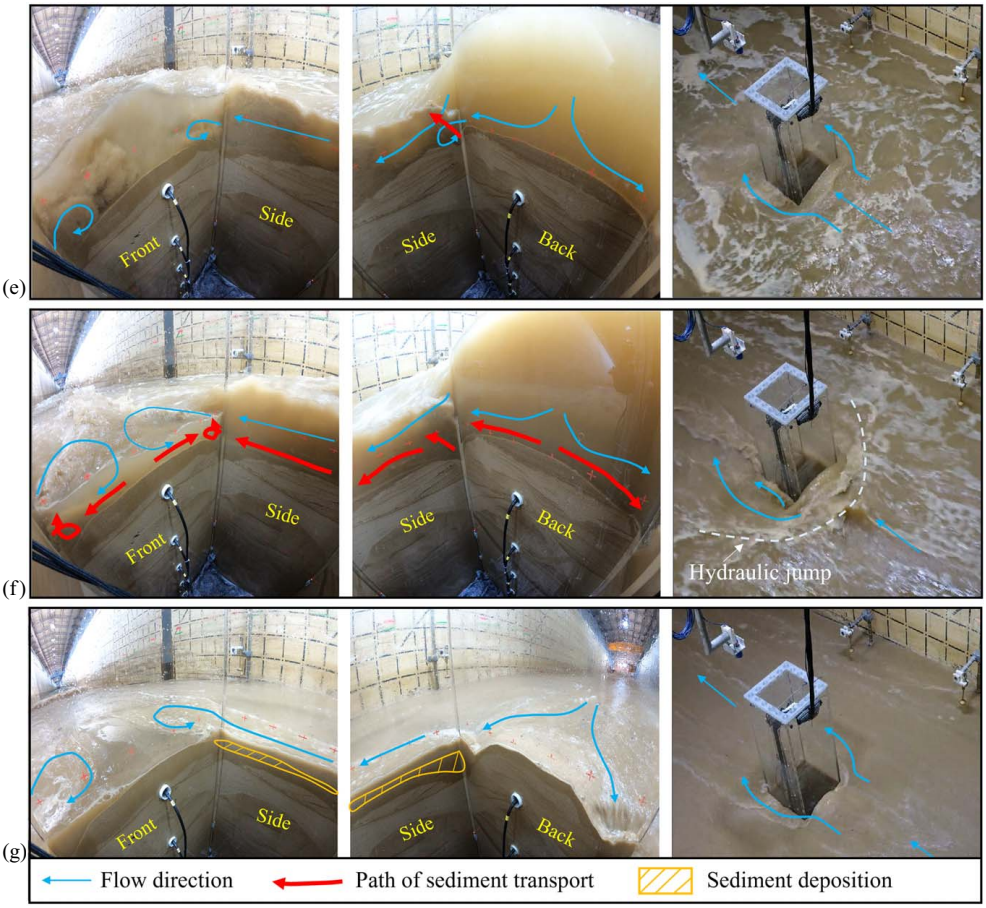

Fig. 6. (*Continued.*)

face of the column were also observed by Tonkin et al. (2003), although for a round cylinder and at the centerline of the back side. In addition to the back side, sediment accumulation also occurred at the lateral face of the column. Here, the sediment settled a few seconds before the sediment at the back face.

Tempospatial Scouring Processes along the Column

To illustrate the scour along the diameter of the square column, the of normalised scour depth (S/D) over time at three sides of the column is shown in Figs. 7–9. Here, the x- and y-coordinates refer to the reference coordinate system introduced in Fig. 1 and the time t starts with bore impact on the column. The scour depth S_{end} depicts the final scour development at the end of a test, whereas the scour depth $S_{reverse}$ describes the bed elevation at the time of flow reversal.

As can be seen in Fig. 7 for Test T01b, immediately after bore impact, the sediment at the two upstream corners [Fig. 7(a) at $y/D =$ 0 and 1] eroded rapidly and distinct scour holes formed in a matter of seconds. The sediment bed in the centerline of the front face did not follow this rapid erosion but scoured in a much slower pace and to a smaller depth, creating a cone-shaped scour profile along the front face [Fig. 7(a)]. The deepest scour profile on the front face occurred near the time of flow reversal. From this extreme point, the scour gradually refilled again during the rundown flow, so that by the end of the test the initial bed level in the centerline [Fig. 7(a) at $y/D = 0.5$] was reached again. The sediment refilling took place over the whole front face, so that a collapse of the scour holes at the corners and sediment slumping as reported by McGovern et al. (2019) is unlikely to be the reason for the refilling.

Along the side face of the column [Fig. 7(b)], the erosion process initially led to an asymmetrical scour profile formed by a deep scour at the upstream [Fig. 7(b) at $x/D = 0$] and minimal scour at the downstream corner ($x/D = 1$). The difference in scour depth between the corners was greatest at the time of flow reversal. After flow reversal, the scour profile along the side face equalized and deepened significantly as sediment was transported from the downstream to the upstream corner. At the end of the test, backfilling led to a substantial reduction in scour depth along the entire side face. Again, as sediment refilling took place along the whole width, sediment slumping from the scour holes at the corners cannot be the single cause. Instead, a large amount of sediment was transported down the sloped beach that settled in the scour hole at the lateral sides of the column. While the locally deepest scour formed at the upstream edge, the overall deepest scour profile was measured during the rundown at $t = 20$ s.

During bore runup, sediment accumulated at the back face of the column [Fig. 7(c)], which was transported there by the return flow from the confluence of the bore downstream of the column [Fig. 6(c)]. With the amplifying rundown flow, scour development on the back face increased abruptly. Similar to the front face during wave runup, the sediment at the corners eroded quickly, resulting in a cone-shaped scour profile. The erosion at the downstream corners [Fig. 7(c) at $y/D = 0$ and 1] was such that the scour depths were at times considerably greater than those at the upstream corners [Fig. 7(a) at $y/D = 0$ and 1]. Despite substantial backfilling at the end of the rundown, especially near the corners, the scour at the downstream corners remained largest until the end of test.

Comparing the development of scour profiles with that of Test T02b (Fig. 8), for which the water level was raised by 20 cm,

J. Waterway, Port, Coastal, Ocean Eng., 2024, 150(3): 04024005

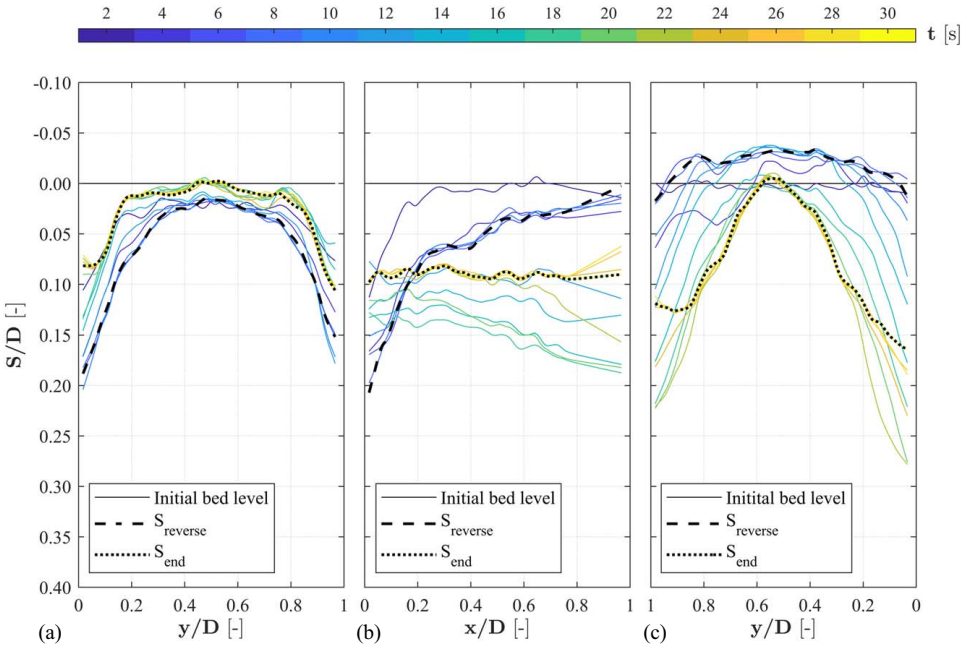

Fig. 7. Test T01b, $H = 0.73$ m, $W = 10$ m. Development of scour depth over time at (a) the front; (b) the side; and (c) the back face of the column.

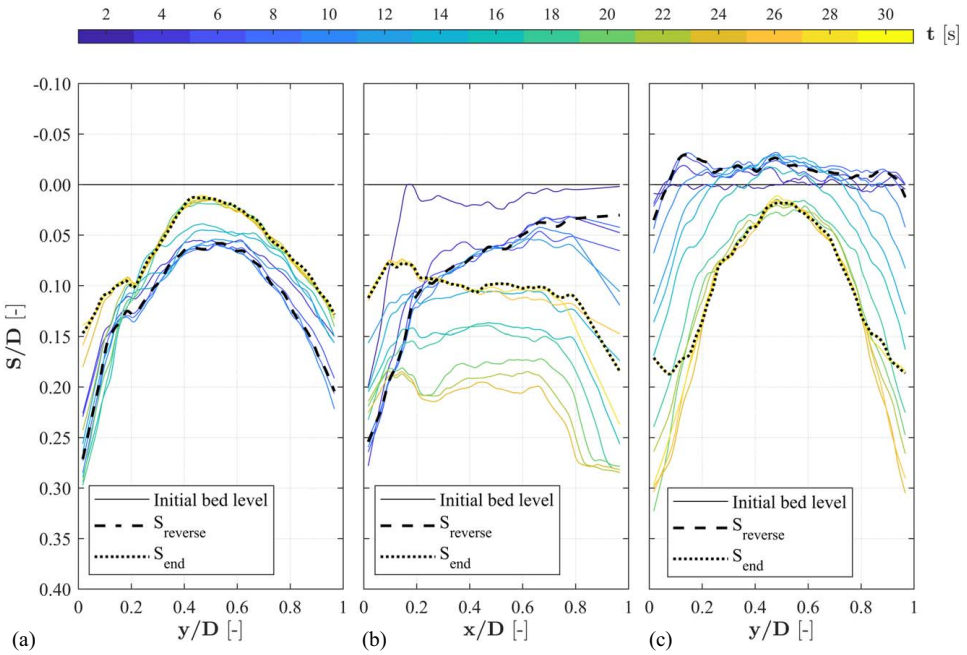

Fig. 8. Test T02b, $H = 0.74$ m, $W = 6$ m. Development of scour depth over time at (a) the front; (b) the side; and (c) the back face of the column.

many similarities can be observed, but also some clear differences. The shape of the scour profiles at the front face of the column was quite similar between the tests, but the general intensity of the scour process was clearly larger in Test T02b [Fig. 8(a)] than in Test T01b [Fig. 7(a)]. The sediment infilling taking place during rundown also reduced the scour depth and the final scour profile was noticeably less deep than at the time of flow reversal. At the side face [Fig. 8(b)], the clearest difference in the scour process manifested. Here, the strong flow during rundown led to a more severe scouring process at the downstream corner of the column [Fig. 8(b) at $x/D = 1$] and prevented the formation of nearly uniform scour depths along the side face as at the end of Test T01b. In addition, the maximum scour depth emerged much later at 25 s after bore impact compared with 20 s in Test T01b. The scour process and development of scour profiles at the back face [Fig. 8(b)] were comparable with Test T01b [Fig. 7(b)] during the bore runup phase, but clearly more pronounced during rundown.

The increased water level in Test T02b implies a reduced distance between column and shoreline. As a consequence, the bore broke closer to the column (6 m instead of 10 m as in Test T01b), resulting in a higher impact momentum of the bore on the column as both flow velocity and flow depth at the column increase. Both the higher flow velocity and the greater flow depth led to the formation of a larger horseshoe vortex. A greater flow

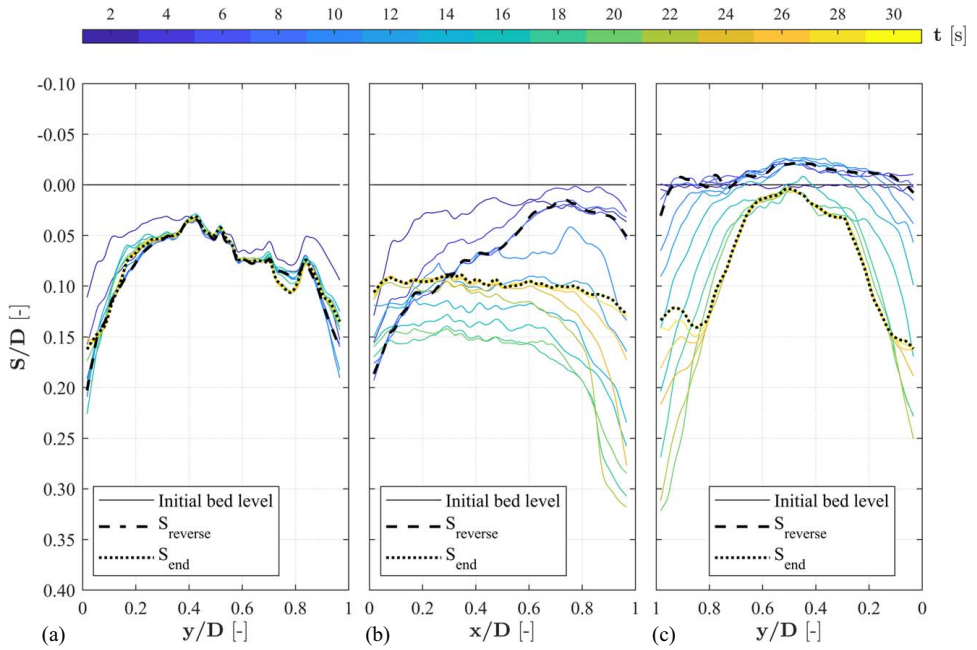

Fig. 9. Test T03, $H = 0.48$ m, $W = 6$ m. Development of scour depth over time at (a) the front; (b) the side; and (c) the back face of the column.

depth allows for a greater thickness of the boundary layer, which in turn can enhance the development of the horseshoe vortex, since the horseshoe vortex is caused by the three-dimensional separation of the boundary layer upstream of the column (Sumer and Fredsøe 2002). At the same time, higher flow velocity leads to a stronger downward flow in front of the column. In conclusion, a higher SWL causes a stronger downward flow and a more pronounced horseshoe vortex. In Test T02b, this leads to a stronger scour formation at the upstream corners of the column compared with Test T01b.

With the more powerful bore impact comes a stronger downward flow and a more pronounced flow separation and vortex formation at the upstream corners, which amplified the scouring process here compared with Test T01b.

Furthermore, the raised water level led to a larger inundation distance on the sloped beach, which gave the rundown flow more distance and time to accelerate, leading to deeper scour at the back face compared with Test T01b.

To illustrate the influence of the initial wave height, Fig. 9 shows the scour development of Test T03, in which the wave height was reduced from 0.74 to 0.48 m compared with Test T02b. Despite the different wave heights, there are similarities in the shape of the scour profiles, particularly on the back and side face of the column. On the back face [Figs. 8(c) and 9(c)], a symmetric cone-shaped scour profile established at the end of the test. In both tests, there was severe scour on the side face of the column at the downstream corner [at $x/D = 1$ in Figs. 8(b) and 9(b)] during the return flow, resulting in a large difference in scour depth on the side face between the downstream and upstream corners. The largest difference is found at the upstream corner, where the scour development during runup was more pronounced in Test T02b [Fig. 8(a) at $y/D = 0$ and also in Fig. 8(b) at $x/D = 0$] than in Test T03 [Fig. 9(a)]. The scour process during rundown, including the sediment infilling at the end of the test, was very similar, which was unexpected. The lowered wave height in Test T03 should have resulted in a smaller wave runup height and inundation distance on the sloped beach, which in turn should have resulted in a reduced load from the rundown flow and, correspondingly, less intense scour on the back face and downstream corners. Instead, the maximum scour depth at the downstream corner [Fig. 9(c) at $y/D = 0$ and 1] was comparable with that in Test T02b [Fig. 8(c)]. A possible indication of reduced flow loading during the rundown is seen at the front face, where the rundown resulted in significantly less sediment accumulation than in the other tests. The scour profile here has hardly changed since the flow reversal.

When comparing the scour profiles with those of McGovern et al. (2019), who showed the evolution of the scour profiles along the front and side face of the column, it is noticeable that the final scour profiles at their front face were more similar to our final scour profiles at the back than at the front face of the column. In the tests presented here, the scour profile at the front face was flatter [e.g., Fig. 9(a) between $y/D = 0.2$ and 0.9] and less conical than that of McGovern et al. (2019), who generated waves with long periods ranging from 25 to 147 s. Here, the wave periods and thus the duration of the wave runup phase were significantly shorter. However, the duration of the drawdown phase in our tests was significantly longer and, at over 20 s, comparable to the wave periods of McGovern et al. (2019). As described in McGovern et al. (2019), this could confirm the clear dependence of the scouring process on the duration of both the runup and the drawdown phase of the wave. Furthermore, as no drawdown was simulated in the experiments of McGovern et al. (2019), the lateral scour profiles differed from those shown here. In the experiments presented here, there was a clear change in the scour profile with reversal of flow direction, whereas the scour profiles in McGovern et al. (2019) deepened continuously but did not change their form.

In summary, two findings can be derived from Figs. 7–9. First, the influence of the distance between column and SWL on the scour development is greater than the influence of the wave height, and second, the scour development during rundown has a greater contribution to the overall scour process than might have been suspected. This is especially true for scour evolution at the side and back face of the column.

J. Waterway, Port, Coastal, Ocean Eng., 2024, 150(3): 04024005

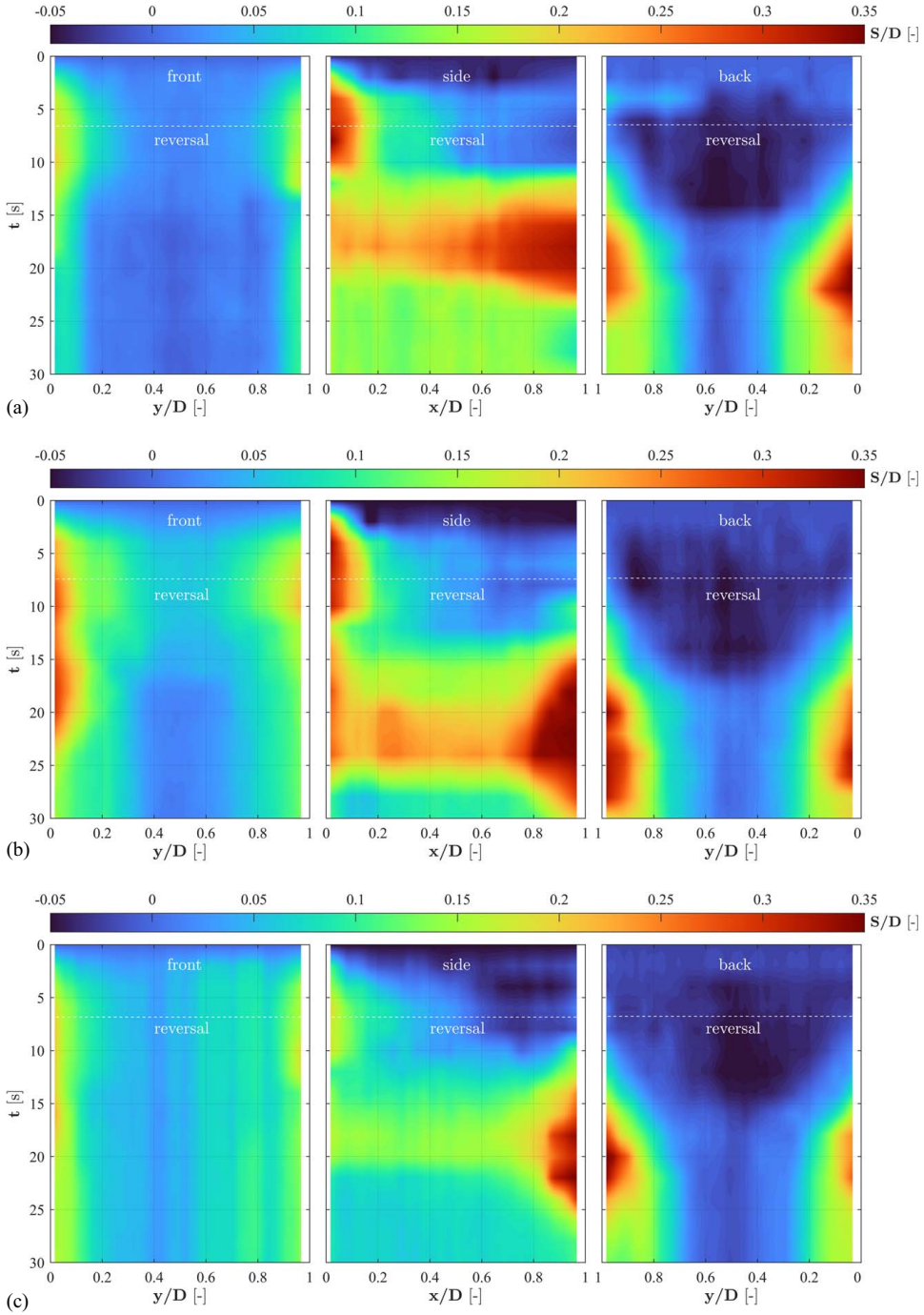

Fig. 10. Scouring pattern interpolated over time and around the three sides of the column for (a) Test T01b; (b) Test T02b; and (c) Test T03.

To demonstrate the variability of scour development over time and in particular the position of the maximum scour depth, Fig. 10 additionally visualizes the scouring process around the column by interpolating the measured scour depths onto a tempospatial scour image. The image consists of the scour depths at all positions around the three faces of the column (x-axis) at every time step (y-axis) that was depicted individually in Figs. 7–9.

From these figures, it can be clearly seen that the largest overall sediment displacement took place on the side face of the column. During the runup phase, the scour process initially developed locally at the upstream corners of the column. With the rundown flow, however, the sediment bed began to move along the entire side face. The scouring process intensified at the downstream corner of the column and eventually exceeded that at the upstream corner, leading to the formation of the maximum scour depth at the downstream corner. On the front and back side of the column, the tempospatial scour pattern was less subject to fluctuations and was almost axis-symmetrical along the respective middle axis. The temporal development of the scour process, however, was reversed. While the initial scour on the front face was partially refilled with the rundown flow, the initial sediment accumulation at the back face had to be eroded by the rundown flow before scour could even emerge in the further course. Altogether, the figures reveal clearly how much the tempospatial scour process directly at the structure is driven by the rundown flow of the returning bore and how the scouring profiles differentiate between the sides of

the column. The scour development and the general mobility of the sediment bed at the structure are significantly more severe during the rundown than during the runup phase.

Development of Scour Depth and Rate over Time

To illustrate the direct dependencies between scour and flow processes, the scour time histories at different positions around the column are plotted against flow parameters in Fig. 11, using Test T03 as an example. The time history of the flow parameters presented in this figure, depth-averaged flow velocity $\bar{U}$, flow depth h, and Fr number, were obtained using the FLOW-3D model. Owing to the mostly axisymmetric scour pattern (cf. Figs. 9 and 10) and for reasons of clarity, the selection of points is limited to two per side. For each side, the scour development is shown in the center and at one corner. The time history starts with $t = 0$ s as the time of impact of the wave on the column.

At the front (offshore) corners of the column, the scour process started immediately after wave impact and reached a large scour depth during the runup phase. Interestingly, the scour at the center of the front side [position of the diamond in the inlet of sub Fig. 11(a)] was much less severe than that at its corners (position of the square). A delay in the progression of scour in the center of the front compared with the corners was reported by McGovern et al. (2019) and Mehrzad et al. (2022). McGovern et al. (2019) attributed the initial delay in the centerline scour development to a weaker horseshoe vortex in the early stages of the scour process. Tonkin et al. (2003) reported a rapid progression of scour along the entire front of their cylinder due to the strong horseshoe vortex induced by the plunging breaker. In this study, however, the influence of the horseshoe vortex on the front scour process seems to have been outweighed by flow separation and vortex shedding at the front corners. After flow reversal, during which the flow and thus the scouring process stopped, the scour depth remained almost constant at the front. Considering all sides of the column, the maximum scour depth during the runup phase always remained at the two front-facing (offshore) corners. The scour development on the lateral side [position of the "x" in the

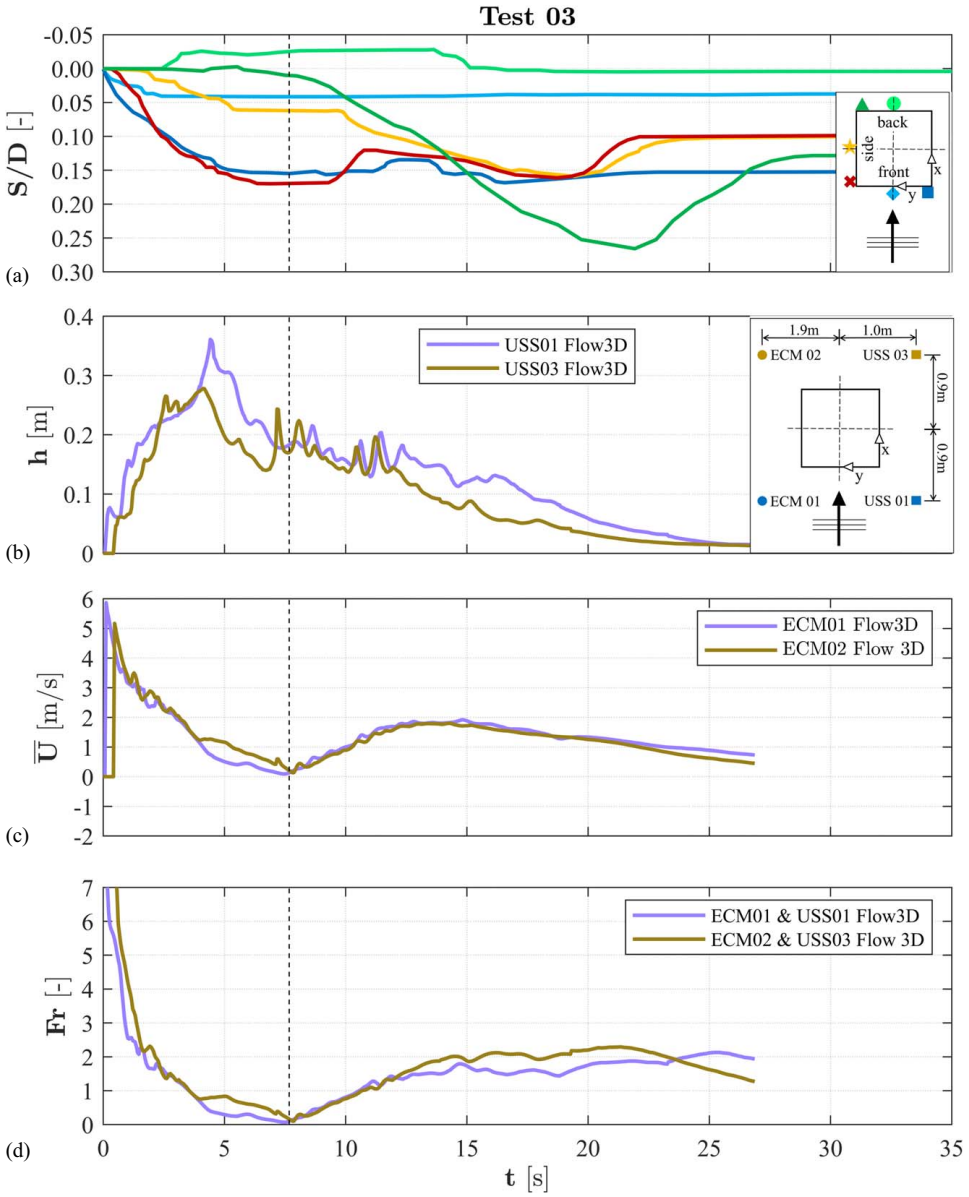

Fig. 11. (a) Scour development over time at selected points around the column. Dashed line represents time of flow reversal at the column; (b) flow depth; (c) flow velocity; and (d) Froude number were obtained by FLOW3D simulation.

J. Waterway, Port, Coastal, Ocean Eng., 2024, 150(3): 04024005

inlet of sub Fig. 11(a)] of the front corner was very similar to its front-facing counterpart (position of the square). The main differences were a delay in the onset of scour development during the runup phase and a more pronounced refilling of the scour hole during the drawdown phase.

At the centerline of the lateral face [position of the star in the inlet of sub Fig. 11(a)], the development of the scour was completely different from that of the front face. In contrast to the front face and the front corner, there was a delayed and significantly slower scour development during the runup phase. However, the drawdown phase caused a second and stronger scouring phase, which ended in backfilling to the level of the front corner. In general, the scour at the side of the column follows the same progression as described by Tonkin et al. (2003). While Tonkin et al. (2003) observed large scour development during the drawdown phase, it did not match the extent of the runup phase at this particular location. However, in this study, the contribution of scour during the drawdown phase to the total scour at the end of the test is greater than that of runup scour. This confirms the perception that the rundown phase has a much greater influence on the overall scour development than described in previous studies.

The scour development at the rear of the column followed a different sequence of phases. During the runup phase, sediment was initially deposited by water flowing back from the confluence point behind the column [Fig. 6(c)]. With the onset of the drawdown phase, the scour depth at the back (onshore) corner increased steadily until, toward the end of the test, a large part of the previous scour hole was refilled. As a result of this sediment infilling, the final relative scour depths at the end of the test were significantly reduced compared with the maximum scour depth measured during the test.

As can be seen from Fig. 11, the position of the maximum scour depth changed from the front to the back side during the test, similar to what has been reported for tidal current-induced scour (Schendel et al. 2018). The time history of the scour also suggests that the flow processes led to a locally stronger scour development during the drawdown phase than during the runup phase.

To provide additional insight into the reasons for the differences in scour progression during runup and drawdown, Figs. 12 and 13 show the physical scour rate at the front and back corners of the column for Test T01b and Test T03, respectively. A negative scour rate indicates refilling of the scour hole. At the front corner (position of the square in the inlet of Figs. 12 and 13), the scour rate was highest immediately after the wave impact on the column. During the runup phase, the scour rate then decreased continuously toward zero at the time of flow reversal.

The peak scour rate at the beginning was greater in Test 01b (Fig. 12) than in Test 03 (Fig. 13). On the one hand, the wave impact should have been less in Test 01b given the greater distance between the column and the shoreline. The flow velocities predicted by the Flow 3D model upstream of the column at this time are greater in Test 03 and would indeed suggest faster scour development in Test 03. On the other hand, the wave height in Test 03 was considerably smaller than in Test 01b, which should result in a higher load in the latter. Comparing Test 03 and Test 01b, it appears that the height of the wave is equally as important as the distance from the column to the shore in determining the rate of scour at the start of the runup phase. However, the values of the scour rate as a gradient between two measurements are sensitive to the interval between the two measurements, which was not the same between the two tests.

At the back corners of the column (position of the triangle in the inlet of Figs. 12 and 13), the scour rate remained close to zero or even slightly negative. A positive scour rate could only be measured just before the end of the runup phase. During the subsequent drawdown phase, the behavior changed and the scour rate at the back of the column was continuously higher than that at the front, although the maximum scour rates at the beginning of the runup phase were not reached again. While the maximum amplitude of the scour rate was smaller during the drawdown phase, a positive scour rate was present for a longer period of time than during the runup phase, ultimately leading to a more severe scour process on the back side. Therefore, in addition to the amplitude of the load, its duration plays an important role in the scouring process. The duration in which the flow velocity surpassed the critical velocity ($u_c = 0.30$ m/s) of the sediment was significantly longer during the drawdown than during the runup phase. For Test 3 (Fig. 11), the period of $\bar{U} > u_c$ amounted to 6.3 s during the runup phase, whereas u_c was exceeded for around 20 s in the drawdown phase.

Sumer et al. (2011) showed for a plunging solitary wave that large bed shear stresses can occur during drawdown for a significantly longer period than during runup. The bed shear stresses during the drawdown phase are generated by the turbulent boundary layer of the descending flow. Driven by these bed shear stresses, large scour and sediment transport are expected, eventually leading to scour refilling at the end of the drawdown phase, as indicated by the negative scour rates at the 23 s mark in Figs. 12 and 13.

For the back of their cylinder, Tonkin et al. (2003) reported a similar evolution of scour rates, that is, small scour rates at the beginning of the test and increasing rates during the drawdown phase until negative scour rates indicated refilling toward the end of the test.

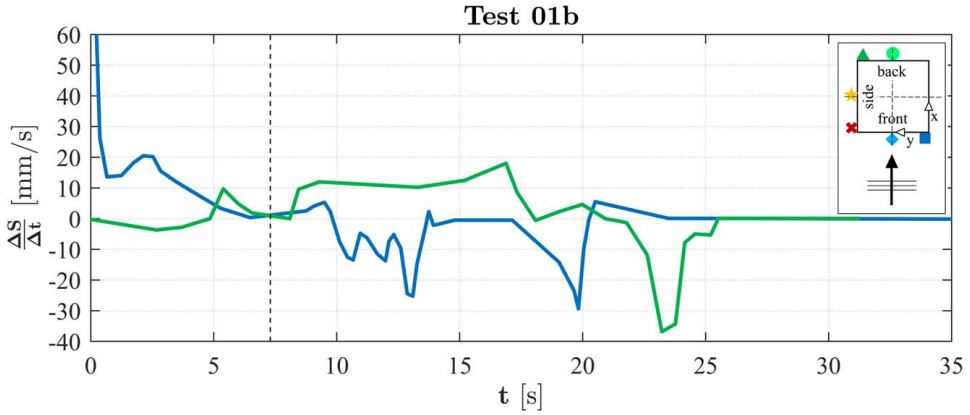

Fig. 12. Scour rate at the front and back edges over time for Test T01b.

J. Waterway, Port, Coastal, Ocean Eng., 2024, 150(3): 04024005

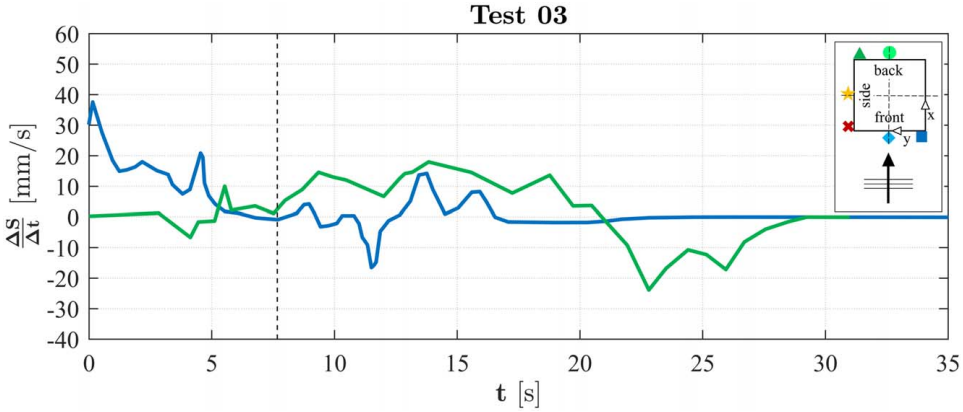

Fig. 13. Scour rate at the front and back edges over time for Test T03.

Comparison of Scour Development over Time in Dependency to SWL Distance and Wave Height

To demonstrate the impact of wave height and column distance from the SWL on the scour development, tests with either similar initial wave heights (Tests T01b, T02b, and T05) or similar distances from the SWL (Tests T02b, T03, and T04) were compared. The runup behavior of the wave on the beach changes with wave height and water level. As a result, the duration of the runup and drawdown phases differs between the tests. To enable a comparison of the scour development over time between tests, the time histories in the following figures are thus centered on the time of flow reversal.

To demonstrate the influence of the distance between the column and the SWL, Figs. 14 and 15 illustrate the scour development over time at both the front (Fig. 14) and the side face (Fig. 15) of the column. As expected, the intensity of the scouring process at the front of the column [Fig. 14(a)] increased as the distance to the SWL decreased. With decreasing distance, the wave hit the column with increasing flow depth h [Fig. 14(b)] and increasing flow velocity $\bar{U}$ [Fig. 14(c)], resulting in a larger momentum flux M [Fig. 14(d)] during the runup phase. As previously mentioned, a pronounced surface roller has formed at the front face of the column during the runup phase [Fig. 6(b)]. As described by Melville (2008), a surface roller rotates in the opposite direction to the horseshoe vortex and can weaken it when the two vortices interfere. As the flow depth decreases, the surface roller becomes more dominant and its weakening effect on the horseshoe vortex may increase, leading to a reduction in scour depth. However, it is likely that the weakening effect caused by the surface roller is only an added factor to the overall impact of water depth to the formation of the horseshoe vortex. As water depth decreases, the boundary layer reduces, leading to a smaller horseshoe vortex and thus a smaller scour depth. Unfortunately, owing to high levels of turbidity and turbulence, the interaction between the surface roller and the horseshoe vortex could not be observed in the video recording. Any possible additional weakening of the horseshoe vortex by the surface roller at shallow water depths is therefore an interpretation by the authors based on descriptions in Melville (2008).

At the side face (Fig. 15), the difference in scour depth was even more pronounced than at the front face. Here, the horseshoe vortex may only be an indirect driver of the scour process. As observed in the videos from the inside of the column and indicated in Fig. 6 for Test 03, the scour at the corners of the column was mainly driven by a strong vortex generated by the lateral separation of the boundary layer from the edge of the structure. From there, the scour continued along the side of the column. In part, these lateral eddies are driven by the horseshoe vortex at the front of the column, which trails from the center to the edges. A larger flow depth could therefore also lead to a larger scour depth at the side of the column. However, the strength of the lateral vortices is more likely to be controlled by the runup flow velocity and the deflection of the flow toward the edges.

Figs. 16 and 17 compare the scour development between tests with different wave heights. The water level in these tests was identical, so the nonlinearity parameter varied between the tests. As expected, a greater wave height resulted in greater flow depth [Fig. 16(b)], flow velocity [Fig. 16(c)], and consequently greater momentum flux [Fig. 16(d)] during the runup phase. In contrast to the change in distance between column and SWL (Fig. 15), there was no significant change in scour development due to the difference in wave height at the side face of the column [Fig. 16(a)]. Only toward the end of the drawdown phase, a noticeable distinction in the scour process becomes apparent. This difference is likely to be caused by a difference in runup height and effective inundation period, which is the time in which the effective bed shear stress exceeds the critical shear stress of the soil according to McGovern et al. (2019). A large wave height leads to a high runup height on the sloped beach. During the subsequent drawdown phase, the high runup transfers into a large flow velocity [Fig. 16(c)], which also acts for a long period of time. As a result, bed shear stresses larger than the critical threshold are sustained over a long duration, leading to larger scour depth during drawdown with increasing wave height.

At the upstream edges of the front face (Fig. 17), scour depth clearly increased with wave height, even during the runup phase. During the drawdown phase, a higher wave height resulted in greater backfilling. In the test with the lowest wave height (Test 03), no backfilling was observed [Fig. 17(a)]. In summary, the findings reveal that under the tested boundary conditions, the distance of the column from the SWL, and hence the wave breaking point, has a much greater influence on the scour development than the height of the wave.

Comparison of Final and Maximum Scour Depth

The results so far have shown that the final scour depth around the column at the end of a test can be significantly less than the maximum scour depth during the test. On the one hand, the backflow during the drawdown phase led to a renewed intensification of the scour process, and on the other hand, the scour hole was refilled at the end of the drawdown. As mentioned at the beginning of this

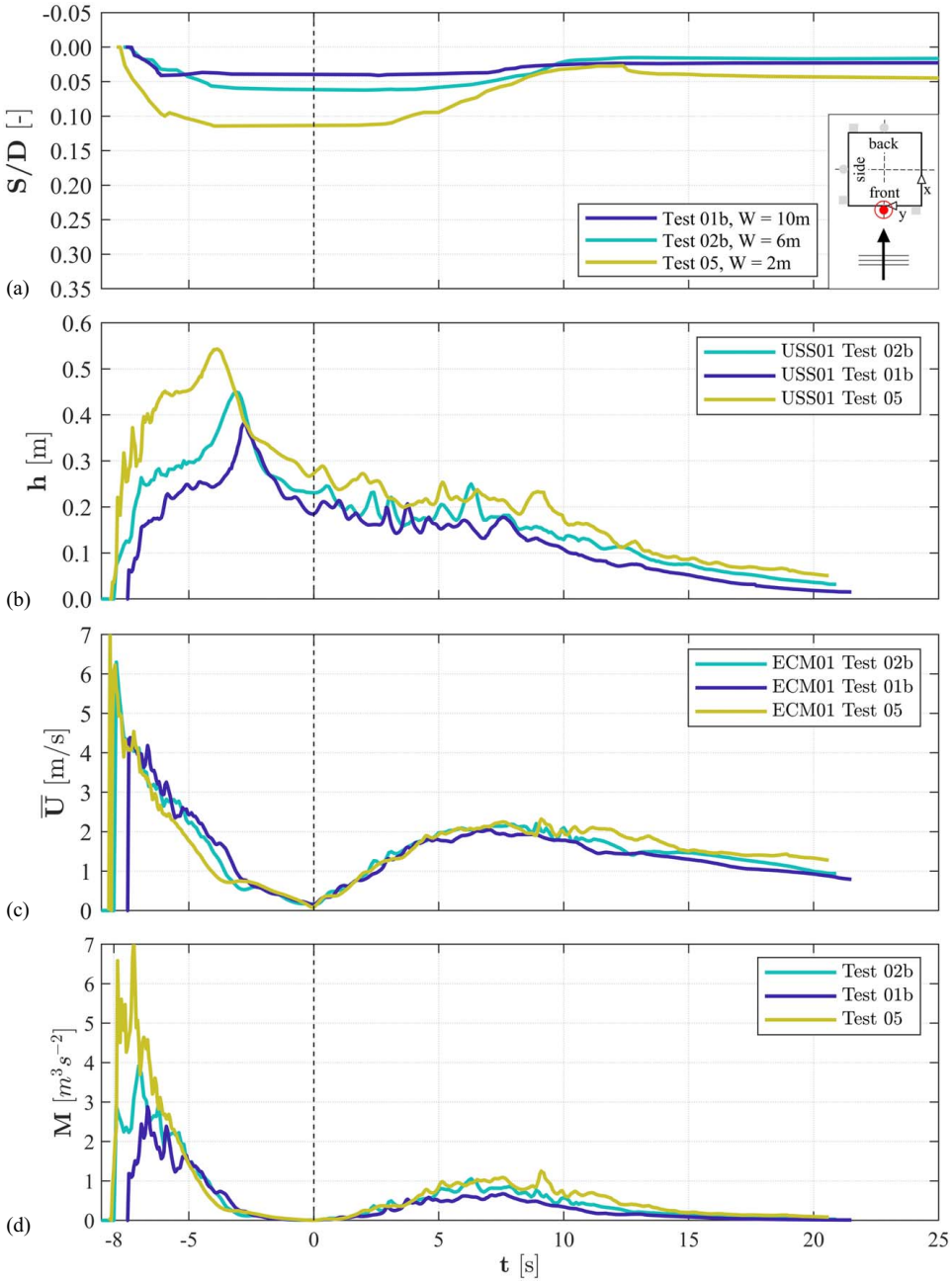

Fig. 14. Influence of distance from shore on (a) scour development at the front; (b) flow depth; (c) flow velocity; and (d) momentum flux for tests with similar wave height. Distance from shore for Test T01b = 10 m, for Test T02b = 6 m, and for Test T05 = 2 m.

paper, the exact determination of this discrepancy in scour depths can be quite important for the formulation of reliable design guidelines, especially since the results of field studies cannot account for this discrepancy. Therefore, the differences between the final (S_{end}) and maximum (S_{max}) scour depths will be discussed in more detail in this section. This will be done by comparing them with the influences of individual hydraulic boundary conditions as illustrated in Fig. 18. In addition to the final and maximum scour depth, Fig. 18 shows the maximum scour depth at the end of the runup phase, $S_{reverse}$, to indicate the proportion of the runup phase on the maximum scour depth.

The clearest correlation between S_{end} and S_{max} is found as a function of distance from the SWL (W). From Fig. 18(a) it can be seen that both scour depths decreased at similar rates as the distance of the structure from the SWL increased. In relative terms, represented by the ratio S_{max}/S_{end} [dashed line in Fig. 18(a)], the difference between the two scour depths increased slightly with increasing distance. Conversely, this means that the further away the structure is from the SWL, the more of the scour will be backfilled during the drawdown.

On the other hand, the scour depth caused by the runup alone, $S_{reverse}$, decreased significantly with increasing distance of the column from the SWL [Fig. 18(a)]. Thus, the influence of the distance between column and SWL on the scour process was more pronounced during runup than during drawdown. This makes sense as the scour process during runup is determined by the impact of the wave on the column, which increases the closer the column is to the shoreline. Yeh et al. (2001) also found a smaller scour

J. Waterway, Port, Coastal, Ocean Eng., 2024, 150(3): 04024005

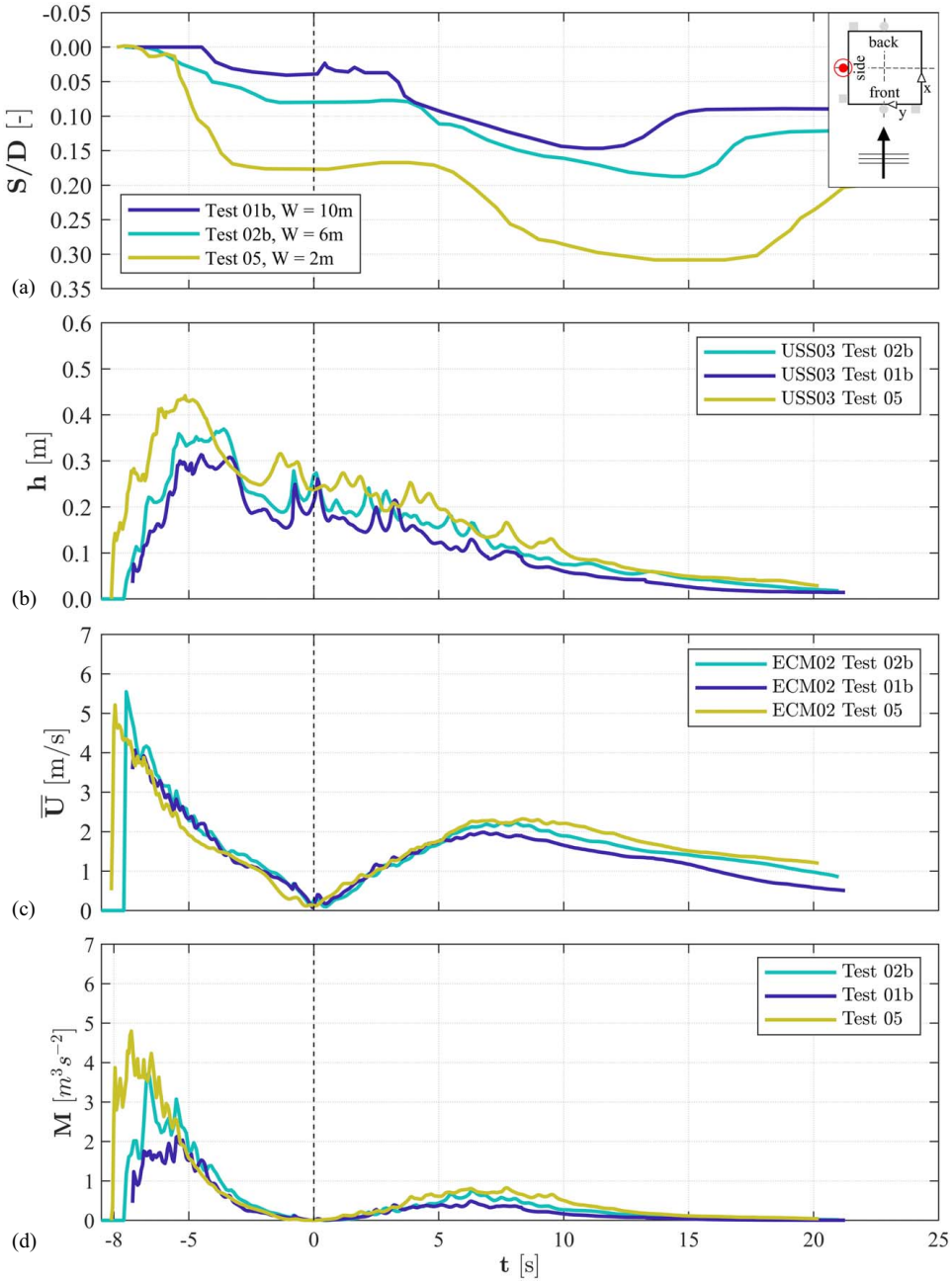

Fig. 15. Influence of distance from shore on (a) scour development at the side; (b) flow depth; (c) flow velocity; and (d) momentum flux for tests with similar wave height. Distance from shore for Test T01b = 10 m, for Test T02b = 6 m, and for Test T05 = 2 m.

depth around a cylinder that was placed inshore than around one that was placed at the SWL. They suggested that the energy dissipation of the wave during the runup over a dry bed before reaching the structure was a possible explanation. Overall, it appears that with increasing distance W, the contribution of the runup scour to the maximum scour depth decreases and the influence of the drawdown phase on the maximum scour depth increases.

Fig. 18(b) compares the different scour depths with the wave height. The correlation of scour depth, especially the maximum scour depth S_{max}, with the wave height H was weaker than with the distance between column and SWL. However, there was a general trend of increasing scour depth with increasing wave height. Setting aside the substantial scour depth observed in Test 03 at $H/D = 0.8$ for now—this case will be further discussed later—the difference between the final (S_{end}) and maximum scour depths (S_{max}) appears to increase with increasing wave height, akin to the influence of the distance W. Employing the same line of reasoning as earlier, this implies that as the wave height increases, a larger portion of the maximum scour is refilled.

As the increase of $S_{reverse}$ with wave height was less steep than that of S_{max}, the influence of runup on the overall scour process appears to decrease with increasing wave height [Fig. 18(b)].

Finally, Fig. 18(c) compares the scour depths with the maximum inundation depth h_{max}. The final scour depth S_{end} followed a clear trend of increasing scour depth with increasing inundation height. In this study, the maximum inundation depth is defined as the maximum flow depth calculated by the Flow 3D model at the position of USS01, 90 cm upstream of the center of the column. An increase in scour depth with increasing inundation depth is consistent with the results of previous studies (e.g., Mehrzad

J. Waterway, Port, Coastal, Ocean Eng., 2024, 150(3): 04024005

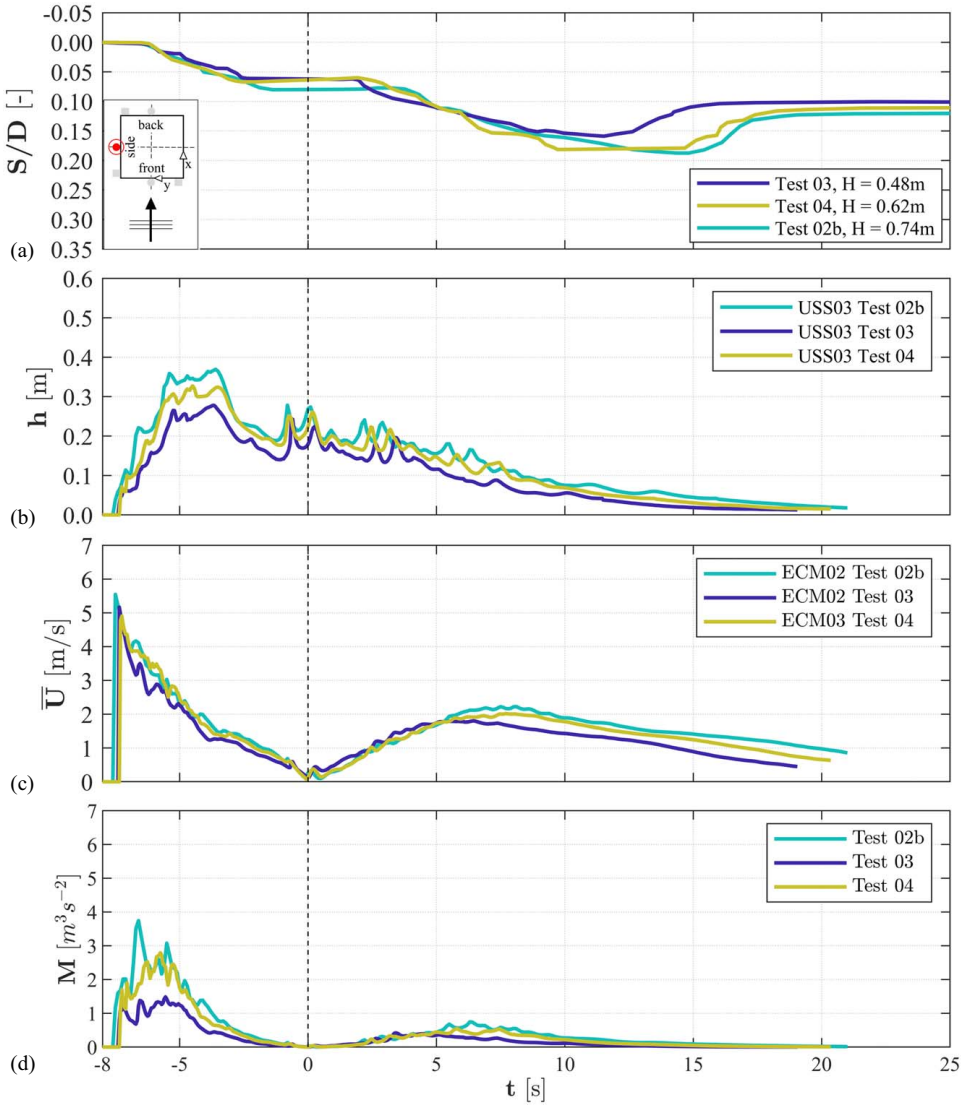

Fig. 16. Influence of wave height on (a) scour development at the side; (b) flow depth; (c) flow velocity; and (d) momentum flux for tests for tests with similar distance from shore. Wave height for Test T02b = 0.74 m, for Test T03 = 0.48 m, and for Test T04 = 0.62 m.

et al. 2022) and corresponds to the basic expectation that a greater flow depth leads to a greater scour depth.

However, as can be seen from Fig. 18(c), it is more difficult to identify a clear trend for the maximum scour depth S_{max}, as an unexpected large maximum scour depth was measured in Test 03, despite the low inundation depth during this test. Given the conditions of Test 03, that is, low resulting flow depth and flow velocity, as shown in Figs. 16 and 17, a lower equilibrium scour depth would have been expected than in the comparable Tests 02b and 04. This is true for both the runup and the drawdown phases. If the scour process is simplified and compared with that in steady flow conditions, the time scale for reaching this equilibrium scour depth should be dependent on the boundary layer thickness and the Shields parameter (Sumer et al. 1992). Correspondingly, the time scale should decrease with decreasing flow depth, but increase with decreasing Shields parameter, although the Shields parameter again depends on the flow depth. Therefore, the scour process may be more advanced (greater proportion of equilibrium scour depth reached) during drawdown in Test 03 than in Tests 02 and 04.

McGovern et al. (2019) also observed an increase in scour depth for small inundation depths. They concluded, in agreement with Nakamura et al. (2008), that the effective inundation period can have a greater influence on the scour development than the inundation depth. In their study, tests with a shallow inundation depth still resulted in a large scour depth because the duration of the tests was long enough to allow a fully established flow field and scour process during the inundation time.

Test 03 does not show a similar connection with the inundation time. Of all the tests, Test 03 had the smallest wave height and the smallest nonlinearity parameter. Accordingly, a small wave runup height (Synolakis 1987) and consequently a small inundation time, which in our case is the combined duration of runup and drawdown, should be expected. The scour time histories shown in Fig. 16(a) confirm that the scour process stopped earlier in Test 03 than, for example, in Test 04. Therefore, at the time of writing, the reason for the large maximum scour depth in Test 03 is unclear. However, it should be noted that the measured scour depths are subject to some uncertainty due to the high turbulence and turbidity of the water phase. In addition, the final scour profile at the offshore face of the column in Test T03 shows a less symmetrical scour hole (cf. Fig. 9) than in other tests.

Fig. 19 directly compares the maximum and final scour depths, as well as the scour depth at the time of flow reversal. The comparison also includes scour depths from previous studies using either a

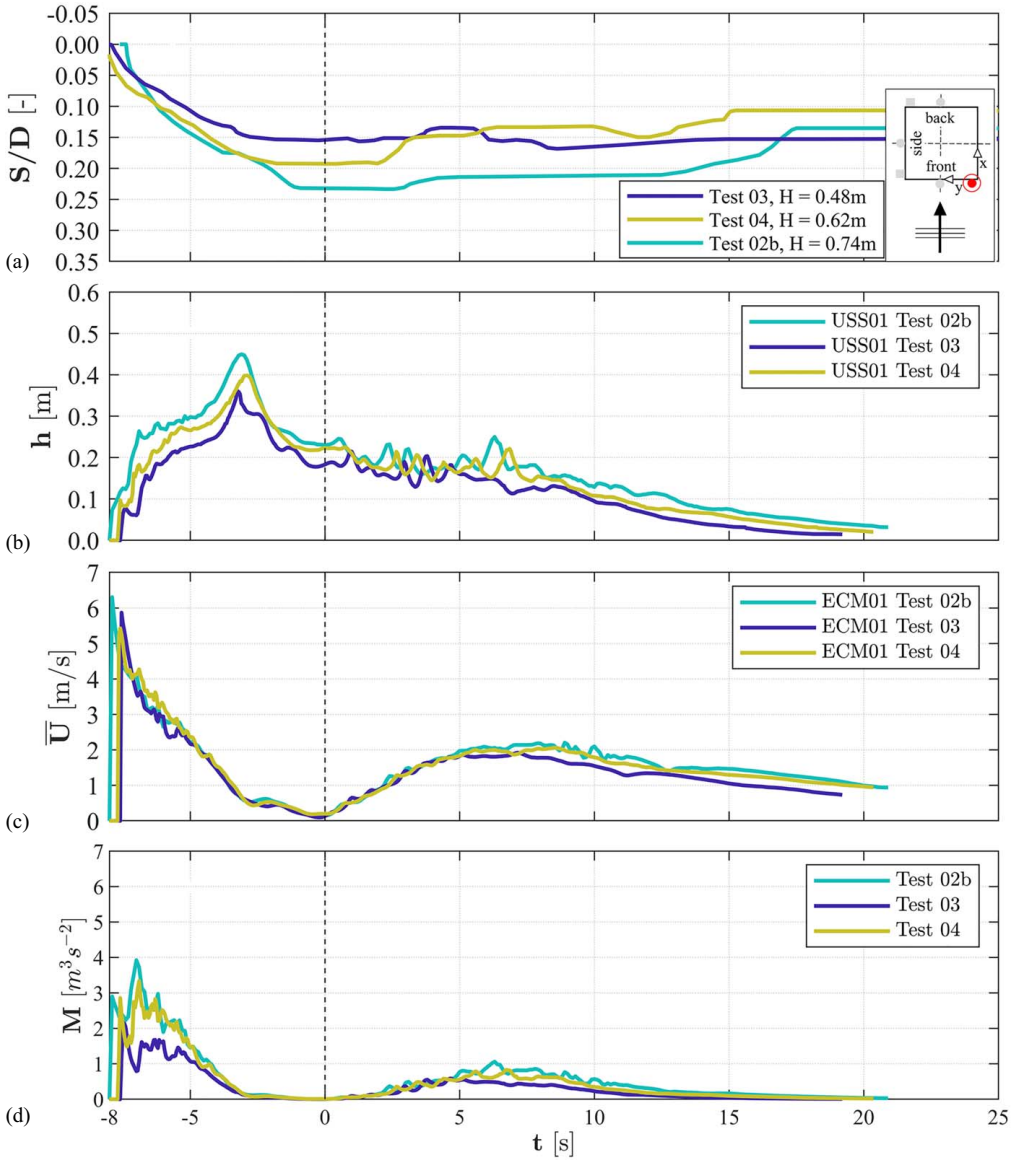

Fig. 17. Influence of wave height on (a) scour development at the front edge; (b) flow depth; (c) flow velocity; and (d) momentum flux for tests for tests with similar distance from shore. Wave height in Test T02b = 0.74 m, for Test T03 = 0.48 m and for Test T04 = 0.62 m.

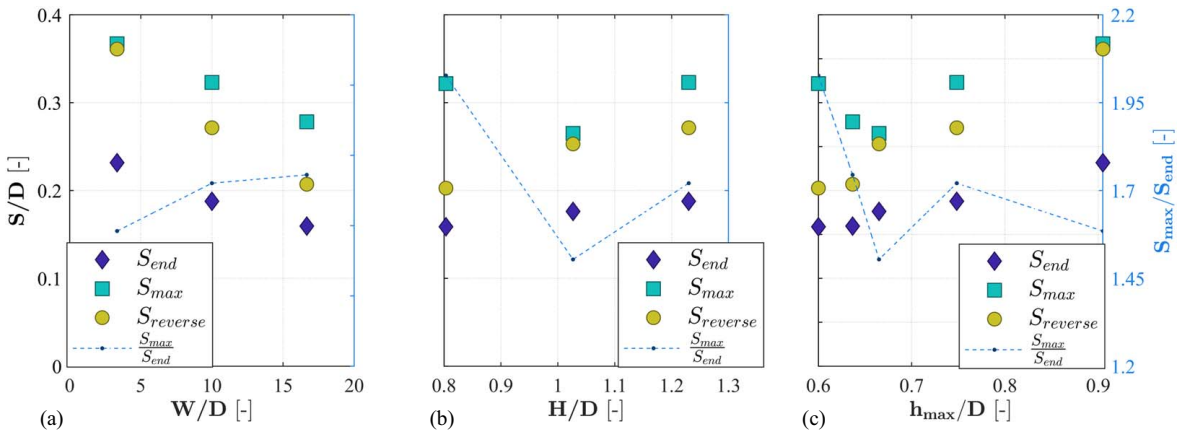

Fig. 18. Left y-axis: comparison of maximum S_{max} and final scour S_{end} depth in (a) dependency to distance from shore W; (b) to wave height H; and (c) to maximum inundation depth h_{max}. Right y-axis: dependency of ratio S_{max}/S_{end} on maximum inundation depth h_{max}, wave height H, and distance from shore W.

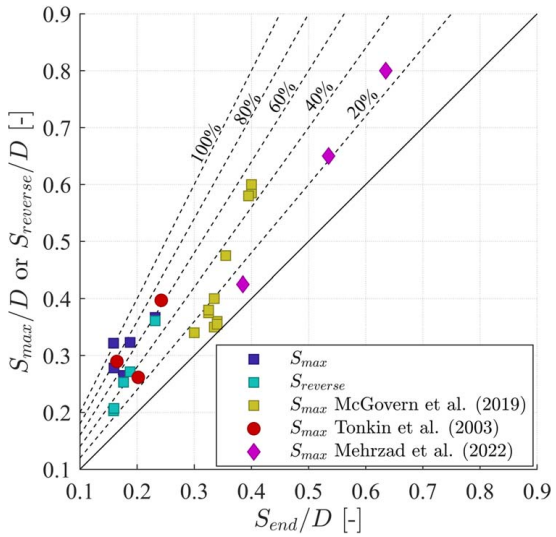

Fig. 19. Comparison of final scour depth S_{end} with overall maximum scour depth S_{max} and maximum scour depth at instant of flow reversal $S_{reverse}$.

similar square column (McGovern et al. 2019; Mehrzad et al. 2022) or a similar sloped beach (Tonkin et al. 2003). As a result of sediment infilling during the drawdown phase, the maximum scour depths achieved during the drawdown phase were up to 100% greater than the final scour depths at the end of the tests.

This discrepancy between final and maximum scour depths was much greater than previously reported. For a horizontal sediment bed, McGovern et al. (2019) reported that maximum scour depths were up to 50% greater than final scour depths. The largest difference between scour depths was found in the tests with the longest wave period and inundation time. Mehrzad et al. (2022) found maximum scour depths up to 25% greater than the final scour depth. The largest difference occurred in the test with the largest bore depth.

Despite the use of a similar square column, it is difficult to compare the scour depth with these studies, as no actual infilling by sediment transport was responsible for the reduction in scour depth but scour hole slumping occurred in both studies. But even in the study of Tonkin et al. (2003), where considerable sediment transport and scour hole infilling at the end of the drawdown phase was reported, only differences between final and maximum scour depth of up to 76% were found. However, it is evident that the difference between maximum and final scour depths is greater in studies where wave drawdown occurs. This suggests that there is significant sediment transport and scour hole infilling due to offshore-directed sediment transport during water return.

Discussion

As observed in previous studies, backfilling of the scour hole occurred at the end of each test, reducing the scour depth from its maximum value. However, McGovern et al. (2019) observed backfilling due to sediment sliding back into the scour hole at the end of the test, rather than due to sediment carried with the downflow. In their study, the flow velocity decreased so that the horseshoe vortex, but also the vortex shedding at the edge of the column, decreased in intensity toward the end of the wave runup. As a result, there was a lack of support and the steep scour holes collapsed. In contrast, in our test, as shown in Figs. 7–9, sediment backfilling occurred across the entire width, particularly at the front and side faces. Here, the collapse of steep scour holes at the corners cannot be the sole cause of the development of the scour profiles. Instead, a large amount of sediment was transported down the sloping beach and deposited in the scour hole at the front and side of the column already during the drawdown phase. Even at the onshore corners, where the development of the scour profiles looks more like that of McGovern et al. (2019), it is likely to be a combination of sediment transport from outside the scour hole and slumping of the scour hole slopes, as indicated by the start of the refilling process several seconds before the end of the drawdown.

Tonkin et al. (2003), as one of the few studies with a sloping beach, observed a similar refilling of the scour hole around their cylinder at first glance. However, in the center of the onshore side of their cylinder, sediment settlement occurred in less than a second, just before the flow stopped, much faster than the refilling at the edges observed in this study. In addition, in Tonkin et al. (2003), the refilling of the scour hole on the side of the cylinder occurred at almost the same time as on the onshore side. In this study, the refilling on the lateral side always occurred much earlier than on the onshore side face of the column.

Tonkin et al. (2003) attributed the large scour development at the end of the drawdown to the development of pore-water pressure gradients at the back of the pile and the associated reduction in the resistance of the grain structure to erosion. Differences with the results of Tonkin et al. (2003), apart from different wave conditions and the use of a different structure, could be due to a different saturation ratio of the sand. In contrast to Tonkin et al. (2003), the column in these tests was always well above the waterline, which is likely to have resulted in less saturated sand than in the Tonkin et al. (2003) tests. Fig. 3 also shows that the intensity and duration of the wave runup was not sufficient to drive the water deep into the sand wedge. This may also explain the relatively small scour development on the offshore face. During the runup, the water hit dry sand on the offshore face of the column. On the onshore side, the sand had a chance to saturate during the runup, so that the wave hit a partially saturated sand during the drawdown. This difference in the level of soil saturation between the runup and drawdown phases may have favored the scouring process there during the drawdown phase. Overall, owing to the only partial saturation of the soil, it can be assumed that the soil destabilization effect due to pore pressure gradients is rather weak in these tests. Looking at the scour profiles and seeing the largest scour measured at the corners, where potential pore pressure gradients should be smaller than in the center of the offshore face, one could argue the relevance of pore pressure gradients on scour development in this particular setup. Nevertheless, a soil that is not fully saturated and its consequences for pore pressure buildup is a condition that requires more research, as many critical infrastructures exposed to a tsunami event may be located in a similar condition. Studies need to be carried out in which saturation conditions are more systematically controlled and varied.

Finally, this study, and thus the applicability of its results, is limited to breaking solitary waves. The choice of wave parameters and methods for generating tsunamis significantly impacts breaker action and runup behavior. These changes affect energy dissipation and the turbulence level within the flow, which can play a crucial role in scour development. Elevated turbulence levels in the ambient flow have the potential to increase sediment transport and scour around the column. However, in this study, the scour mechanism predominantly arises from flow separation and vortex formation at the square column's corners, generating substantial turbulence. Consequently, it seems unlikely that increased ambient turbulence

directly influences the size of this vortex system or significantly impacts the local scour processes at the structure. Nevertheless, increased turbulence could enhance general sediment transport, introducing additional sediment near the column, potentially decelerating the scouring process. The choice of representing a tsunami by utilizing solitary waves also influences the inundation period and the KC number. Despite acknowledging the limitations, particularly regarding relatively brief inundation periods as outlined by Goseberg et al. (2013), the authors opted to utilize solitary waves in this study. With the primary focus being on the evaluation of wave-induced vortex systems and associated scour formation in a large-scale model setup and given the constraints that come with thus a large model scale, solitary waves were necessary to replicate a tsunami bore scenario. The KC numbers in this study were around 30, significantly lower than those observed in real-scale tsunami waves. At very low KC numbers ($KC < 6$), there is a concern that the flow field around the structure might not endure long enough to sustain a stable vortex system comprising horseshoe and lee-wake vortices. Nonetheless, expected flow structures around the structure were present at some points in time as shown in Fig. 6, suggesting that the KC number was large enough to generate a fully developed vortex system. For larger KC numbers, the horseshoe vortex should become more dominant for the scouring process, compared with lee-wake vortices. McGovern et al. (2019) suggest that during a single inundation, lateral vortexes vortices might dominate the scour mechanism instead of the horseshoe vortex. However, the setup in this study differs from that in McGovern et al. (2019), incorporating the additional influence of a sloped beach. This unique configuration introduces uncertainty regarding the expected magnitude and development of the vortex system. This study marks the first investigation into sloped beaches with square columns, and it remains uncertain whether longer waves align with anticipated vortex systems across different flow regimes. The combination of pressure gradient and shallow flow depth during wave runup, coupled with high ambient turbulence, may not necessarily generate the same vortex system seen in steady flow situations with large KC numbers. Hence, determining the required inundation period for sustained lee-wake vortices and their increased contribution to scour development becomes challenging.

Conclusions

Large-scale experiments on the scour development around a square column on a sloped beach due a broken tsunami bore were carried out. The model tests were unique in the combination of boundary conditions and the level of detail in which the spatiotemporal scour process was recorded and analyzed throughout the entire wave runup and drawdown phase of a tsunami inundation event. Findings regarding the scouring process during the runup and drawdown phase can be summarized as follows:

1. Flow separation and lateral eddies lead to massive scour development at the corners of the column. This applies both to the offshore corners during wave runup and to an even greater extent to the onshore corners during wave drawdown. Toward the end of the drawdown phase, the scour was partially backfilled. The backfilling process was driven by downslope sediment transport induced by sheet flow-like conditions during the drawdown, rather than being the result of collapsing scour holes.
2. The scour profiles along the column were clearly different in shape between each side and changed significantly during the drawdown phase, especially on the lateral side of the column. This resulted in a shift in the position of the scour maximum during the simulated tsunami event from the original offshore side to the onshore side, potentially placing an additional semi-dynamic load on the structure.
3. The temporal scour process went through a different sequence of phases on the different sides of the column. At the front, a strong scour phase during the wave runup was followed by a stagnation of the scour process at the time of the flow reversal, followed by a refilling of the scour hole during the wave drawdown. In contrast, on the lateral side of the column, a second strong scour phase occurred after the flow reversal, before the scour was again refilled at the end of the drawdown. At the back of the column, the scour process started with an accumulation of sediment, which was eroded when the reverse flow commenced. The subsequent massive scour phase was also followed by a refilling of the scour at the end of the drawdown.
4. Overall, the drawdown phase added up to 58% to the scour depth obtained during the wave runup alone, $S_{reverse}$, which, as expected, decreased significantly with increasing distance of the column from the SWL. This confirmed the perception that the drawdown phase can have a much greater influence on the overall scour development than described in previous studies.
5. As a result of sediment infilling during the drawdown phase, the maximum scour depths S_{max} achieved during the drawdown phase were up to 100% greater than the final scour depths S_{end} at the end of the tests, which is a significantly larger discrepancy than found in previous studies using a flat sediment bed. The strongest correlation between S_{end} and S_{max} was found as a function of the distance of the structure from the SWL (W), where the difference between the two scour depths increased slightly with increasing distance. The correlation of maximum scour depth S_{max} with wave height H was weaker.

The study illustrated the large variability in the intensity of the transient scour process and the evolution of scour depths around the structure during the course of a tsunami inundation. It was shown that the return flow is responsible for a second, sometimes even more intensive scour phase and that this can lead to a large discrepancy between the final and maximum scour depth. Therefore, the hydrodynamic boundary conditions of the wave drawdown phase should also be considered when formulating resilient design principles for coastal structures that take scour into account.

Data Availability Statement

All data supporting the findings of this study are available from the corresponding author upon reasonable request.

Acknowledgments

The authors would like to acknowledge the support of everyone who assisted with the laboratory experiments reported here, in particular Matthias Kudella, Martin Miranda-Lange, Jörg Hanekop, Kay Jürgensen, Jens Mennenga, and Jens Müller of the Coastal Research Center. The authors would also like to thank the following students for their assistance with the experiments and data preparation: Hannah Fooken, Alisha Friedrichs, Jens Goldenstein, Malte Kumlehn, Maximilian Behnke, Mareile Wynants, Zuwei Li, Élise Fredebohm, Elin Schuh, Fabian Portz, Leon Vinkelau, and Lisa Holste. Finally, Alexander Schendel gratefully acknowledges the support of the German Federal Ministry for Economic Affairs and Climate Action within the funded project "marTech" (BMWK: 0324196A-B).

References

April-LeQuéré, P., I. Nistor, A. Mohammadian, S. Schimmels, A. Schendel, N. Goseberg, M. Welzel, C. Krautwald, and J. Stolle. 2022. "Hydrodynamics and associated scour around a free-standing structure due to turbulent bores." *J. Waterw. Port Coastal Ocean Eng.* 148 (5): 04022013. https://doi.org/10.1061/(ASCE)WW.1943-5460.0000717.

ASCE. 2022. *Minimum design loads and associated criteria for buildings and other structures*. ASCE 7-22. Reston, VA: ASCE.

Benjamin Mason, B. H., and H. Yeh. 2016. "Sediment liquefaction: A pore-water pressure gradient viewpoint." *Bull. Seismol. Soc. Am.* 106 (4): 1908–1913. https://doi.org/10.1785/0120150296.

Bricker, J. D., M. Francis, and A. Nakayama. 2012. "Scour depths near coastal structures due to the 2011 Tohoku Tsunami." *J. Hydraul. Res.* 50 (6): 637–641. https://doi.org/10.1080/00221686.2012.721015.

Gieschen, R., C. Schwartpaul, J. Landmann, L. Fröhling, A. Hildebrandt, and N. Goseberg. 2021. "Large-scale laboratory experiments on mussel dropper lines in ocean surface waves." *J. Mar. Sci. Eng.* 9 (1): 29. https://doi.org/10.3390/jmse9010029.

Goring, D. G. 1978. "Tsunamis—the propagation of long waves onto a shelf." Ph.D. thesis, W. M. Keck Laboratory of Hydraulics and Water Resources Division of Engineering and Applied Science, California Institute of Technology.

Goseberg, N., A. Wurpts, and T. Schlurmann. 2013. "Laboratory-scale generation of tsunami and long waves." *Coast. Eng.* 79: 57–74. https://doi.org/10.1016/j.coastaleng.2013.04.006.

Hoffmans, G. J. C. M., and H. J. Verheij. 1997. *Scour manual*. Rotterdam, Netherlands: A. A. Balkema.

Jayaratne, M. P. R., B. Premaratne, A. Adewale, T. Mikami, S. Matsuba, T. Shibayama, M. Esteban, and I. Nistor. 2016. "Failure mechanisms and local scour at coastal structures induced by tsunami." *Coastal Eng. J.* 58 (4): 1640017. https://doi.org/10.1142/S0578563416400179.

Krautwald, C., et al. 2021. "Engineering lessons from September 28, 2018 Indonesian tsunami: Scouring mechanisms and effects on infrastructure." *J. Waterw. Port Coastal Ocean Eng.* 147 (2): 04020056. https://doi.org/10.1061/(ASCE)WW.1943-5460.0000620.

Larsen, B. E., L. K. Arboll, S. F. Kristoffersen, S. Carstensen, and D. R. Fuhrman. 2018. "Experimental study of tsunami-induced scour around a monopile foundation." *Coastal Eng.* 138: 9–21. https://doi.org/10.1016/j.coastaleng.2018.04.007.

Lavictoire, A. 2014. "Bore-induced local scour around a circular structure." Master's thesis, Dept. of Civil Engineering, Univ. of Ottawa.

McGovern, D. J., D. Todd, T. Rossetto, R. J. S. Whitehouse, J. Monaghan, and E. Gomes. 2019. "Experimental observations of tsunami induced scour at onshore structures." *Coastal Eng.* 152: 103505. https://doi.org/10.1016/j.coastaleng.2019.103505.

Mehrzad, R., I. Nistor, and C. Rennie. 2022. "Scour mechanics of a tsunami-like bore around a square structure." *J. Waterw. Port Coastal Ocean Eng.* 148 (1): 04021048. https://doi.org/10.1061/(ASCE)WW.1943-5460.0000686.

Mehrzad, S., I. Nistor, and C. D. Rennie. 2016. "Experimental modeling of supercritical flows induced erosion around structures." In *Proc., 6th Int. Conf. Application of Physical Modeling in Coastal and Port Engineering and Science*, 1–13. Ottawa, Canada: University of Ottawa.

Melville, B. 2008. "The physics of local scour at bridge piers." In *Proc., 4th Int. Conf. on Scour and Erosion 2008*. Tokyo, Japan: Japanese Geotechnical Society.

Nakamura, T., Y. Kuramitsu, and N. Mizutani. 2008. "Tsunami scour around a square structure." *Coastal Eng. J.* 50 (2): 209–246. https://doi.org/10.1142/S057856340800179X.

Nistor, I., N. Goseberg, and J. Stolle. 2017. "Tsunami-driven debris motion and loads: A critical review." *Front. Built Environ.* 3: 1–11. https://doi.org/10.3389/fbuil.2017.00002.

Nouri, Y., I. Nistor, D. Palermo, and A. Cornett. 2010. "Experimental investigation of tsunami impact on free standing structures." *Coastal Eng. J.* 52 (1): 43–70. https://doi.org/10.1142/S0578563410002117.

Palermo, D., I. Nistor, M. Saatcioglu, and A. Ghobarah. 2013. "Impact and damage to structures during the 27 February 2010 Chile tsunami." *Can. J. Civ. Eng.* 40 (8): 750–758. https://doi.org/10.1139/cjce-2012-0553.

Rivière, N., G. Vouaillat, G. Launay, and E. Mignot. 2017. "Emerging obstacles in supercritical open-channel flows: Detached hydraulic jump versus wall-jet-like bow wave." *J. Hydraul. Eng.* 143 (7): 04017011. https://doi.org/10.1061/(ASCE)HY.1943-7900.0001291.

Schendel, A., N. Goseberg, and T. Schlurmann. 2015. "Experimental study on the erosion stability of coarse grain materials under waves." *J. Mar. Sci. Technol.* 23 (6): 937–942. https://doi.org/10.6119/JMST-015-0610-12.

Schendel, A., A. Hildebrandt, N. Goseberg, and T. Schlurmann. 2018. "Processes and evolution of scour around a monopile induced by tidal currents." *Coastal Eng.* 139: 65–84. https://doi.org/ 10.1016/j.coastaleng.2018.05.004.

Schimmels, S., V. Sriram, and I. Didenkulova. 2016. "Tsunami generation in a large scale experimental facility." *Coastal Eng.* 110: 32–41. https://doi.org/10.1016/j.coastaleng.2015.12.005.

Stolle, J., B. Ghodoosipour, C. Derschum, I. Nistor, E. Petriu, and N. Goseberg. 2018a. "Swing gate generated dam-break waves." *J. Hydraul. Res.* 57 (5): 675–687. https://doi.org/10.1080/00221686.2018.1489901.

Stolle, J., I. Nistor, and N. Goseberg. 2016. "Optical tracking of floating shipping containers in a high-velocity flow." *Coastal Eng. J.* 58: 1650005. https://doi.org/10.1142/S0578563416500054.

Stolle, J., T. Takabatake, I. Nistor, T. Mikami, S. Nishizaki, G. Hamano, H. Ishii, T. Shibayama, N. Goseberg, and E. Petriu. 2018b. "Experimental investigation of debris damming loads under transient supercritical flow conditions." *Coastal Eng.* 139: 16–31. https://doi.org/10.1016/j.coastaleng.2018.04.026.

Sumer, B. M., N. Christiansen, and J. Fredsøe. 1992. "Time scale of scour around a vertical pile." In *Proc., 2nd Int. Offshore and Polar Engineering Conf.* Cupertino, CA: International Society of Offshore and Polar Engineers.

Sumer, B. M., and J. Fredsøe. 2002. *The mechanics of scour in the marine environment*. Edited by B. M. Sumer and J. Fredsøe. London: World Scientific.

Sumer, B. M., M. B. Sen, I. Karagali, B. Ceren, J. Fredsøe, M. Sottile, L. Zilioli, and D. R. Fuhrman. 2011. "Flow and sediment transport induced by a plunging solitary wave." *J. Geophys. Res.* 116: C01008. https://doi.org/10.1029/2010JC006435.

Synolakis, C. E. 1987. "The runup of solitary waves." *J. Fluid Mech.* 185: 523–545. https://doi.org/10.1017/S002211208700329X.

Tonkin, S. P., M. Francis, and J. D. Bricker. 2013. "Limits on coastal scour depths due to tsunami." In *Proc., 6th China–Japan–US Trilateral Symp. on Lifeline Earthquake Engineering*, edited by C. Davis, X. Du, M. Miyajima, and L. Yan, 671–678. Reston, VA: ASCE.

Tonkin, S., H. Yeh, F. Kato, and S. Sato. 2003. "Tsunami scour around a cylinder." *J. Fluid Mech.* 496: 165–192. https://doi.org/10.1017/S0022112003006402.

Whitehouse, R. J. S. 1998. *Scour at marine structures*. London: Thomas Telford.

Yeh, H., F. Kato, and S. Sato. 2001. "Tsunami scour mechanisms around a cylinder." In Vol. 18 of *Proc., Tsunami Research at the End of a Critical Decade*, edited by G. T. Hebenstreit. Dordrecht, Netherlands: Springer. Advances in Natural and Technological Hazards Research.

Yeh, H., and H. B. Mason. 2014. "Sediment response to tsunami loading: Mechanisms and estimates." *Géotechnique* 64 (2): 131–143. https://doi.org/10.1680/geot.13.P.033.

Yeh, H., S. Sato, and Y. Tajima. 2013. "The 11 March 2011 East Japan earthquake and tsunami: Tsunami effects on coastal infrastructure and buildings." *Pure Appl. Geophys.* 170 (6–8): 1019–1031. https://doi.org/10.1007/s00024-012-0489-1.